Analytical and Bioanalytical Chemistry (2019) 411:1839–1862
https://doi.org/10.1007/s00216-019-01593-9

REVIEW

Go with the flow: advances and trends in magnetic flow cytometry

Rita Soares[1,2] · Verónica C. Martins[1,3] · Rita Macedo[1] · Filipe A. Cardoso[1,3] · Sofia A. M. Martins[1,3] · Diogo M. Caetano[2,4] · Pedro H. Fonseca[1,2] · Vânia Silvério[1,2] · Susana Cardoso[1,2] · Paulo P. Freitas[1,5]

Received: 30 September 2018 / Revised: 20 December 2018 / Accepted: 9 January 2019 / Published online: 19 February 2019

Abstract

The growing need for biological information at the single cell level has driven the development of improved cytometry technologies. Flow cytometry is a particularly powerful method that has evolved over the past few decades. Flow cytometers have become essential instruments in biomedical research and routine clinical tests for disease diagnosis, prognosis, and treatment monitoring. However, the increasing number of cellular parameters unveiled by genomic, proteomic, and metabolomic data platforms demands an augmented multiplexability. Also, the need for identification and quantification of relevant biomarkers at low levels requires outstanding analytical sensitivity and reliability. In addition, growing awareness of the advantages associated with miniaturization of analytical devices is pushing forward the progress in integrated and compact, microfluidic-based devices at the point-of-care. In this context, novel types of flow cytometers are emerging during the search to tackle these challenges. Notwithstanding the relevance of other promising alternatives to standard optical flow cytometry (e.g., mass cytometry, various optical and electrical microcytometers), this report focuses on a recent microcytometric technology based on magnetic sensors and magnetic particles integrated into microfluidic structures for dynamic bioanalysis of fluid samples—magnetic flow cytometry. Its concept, main developments, targeted applications, as well as the challenges and trends behind this technology are presented and discussed.

Keywords Magnetic flow cytometry · Magnetic sensors · Magnetic particles · Microfluidics · Point-of-care

Abbreviations

ADC	Analog to digital converter
AMR	Anisotropic magnetoresistance
FM	Ferromagnetic
GMI	Giant magneto impedance
GMR	Giant magnetoresistance
M	Metallic
MACS	Magnetically assisted cell sorting
MFC	Magnetic flow cytometry
MNPs	Magnetic nanoparticles
MR	Magnetoresistance
MRI	Magnetic resonance imaging
MTJ	Magnetic tunnel junctions
PHE	Planar Hall effect
PMTs	Photomultiplier tubes
PoC	Point-of-care
S	Sensitivity
SERF	Spin-exchange relaxation-free
SNR	Signal-to-noise ratio
SV	Spin valve
TMR	Tunneling magnetoresistance
TOF	Time-of-flight

Published in the topical collection *Nanoparticles for Bioanalysis* with guest editors María Carmen Blanco-López and Montserrat Rivas.

Rita Soares and Verónica C. Martins contributed equally to this work.

✉ Verónica C. Martins
vromao@inesc-mn.pt

[1] INESC–Microsistemas e Nanotecnologias (INESC-MN) and IN, Rua Alves Redol 9, 1000-029 Lisbon, Portugal

[2] Instituto Superior Técnico, Universidade de Lisboa, Av. Rovisco Pais, 1049-001 Lisbon, Portugal

[3] Magnomics S.A., Parque Tecnológico de Cantanhede, Núcleo 04, Lote 2, 3060-197 Cantanhede, Portugal

[4] INESC–ID, Rua Alves Redol 9, 1000-029 Lisbon, Portugal

[5] INL, International Iberian Nanotechnology Laboratory, Av. Mestre Jose Veiga, 4715-330 Braga, Portugal

Introduction

Originally described in the first half of the twentieth century [1], flow cytometry has become the gold standard for cellular analysis. It is widely used in life and biomedical sciences to

quickly analyze a large population of cells or particles in a fluid passing on a flow channel, through a detector. The technique allows the analysis of physical and/or chemical characteristics of the target analytes such as size, volume, cycle, and count. In conventional flow cytometry, cell components or particles are labeled by fluorochromes, which emit light at varying wavelengths when excited by a laser. The fluorescent light is filtered and channeled to various photodetectors called photomultiplier tubes (PMTs). These PMT sensors convert the energy of a photon into an electronic signal—a voltage pulse. However, it has been extensively reported that fluorochromes suffer from several limitations, related to background interference, fluorescence noise, stability, and lifetime, which limit the performance of optical flow cytometers. In practice, the potential interference of optical background generated by biological samples often demands extensive sample preparation before sample analysis. Moreover, when using multiple dyes, emission bands are often too broad, causing spectral overlap. This demands compensation for spillover into adjacent detection channels through complex correction algorithms to deconvolute the overlapped spectra. Therefore, alternative technologies to optical flow cytometry have been pursued.

Magnetic flow cytometry (MFC) where the fluorochromes and photodetectors of conventional flow cytometry are replaced by magnetic particles and magnetic field sensors, respectively, is a promising emerging approach. In MFC, magnetically labeled or intrinsically magnetic entities dispersed in a transporter fluid flow inside a channel (often of micrometric dimensions), and pass over a magnetic field sensor (e.g., magnetoresistive, magnetoimpedance, Hall effect). The magnetic sensor detects the magnetic fringe field coming from the flowing magnetic entities (Fig. 1).

An electric-to-electronic coupling is used to record the way in which the magnetically labeled entities flow over the sensor generating information such as particle velocity, labeling density, rotation movement, and particle counts.

A comparative description of the main features of both optical and magnetic approaches is portrayed in Table 1.

Available in a range of sizes and surface functionalization, magnetic labels have important advantages when compared to their fluorophore counterparts. The possibility of particle manipulation and negligible background with respect to biological samples enables the sample's direct electronic readout by appropriate sensors. Indeed, magnetic carriers have become widely used in sample preparation and as a routine methodology for the separation of key cell populations from biological suspensions (e.g., magnetically assisted cell sorting, MACS) [2], which allows single cell analysis. Magnetic cell manipulation is now a standardized process step in numerous processes in laboratory and clinical settings [3].

Different types of magnetic sensors have been explored as transducers in biosensing devices. In the specific case of dynamic detection, a wide range of sensors (e.g., spin valves, magnetic tunnel junctions (MTJ), Hall effect, planar Hall effect (PHE), giant magnetoresistance (GMR)-multilayer sensors, inductive sensors, giant magnetoimpedance (GMI)) have been reported. Their compatibility with microfabrication techniques and microfluidics prompted the development of fully compact, handy, and affordable devices, consistent with the point-of-care (PoC) concept. Indeed, descriptions of MFC systems comprising two to three microfluidic processing zones are emerging in the literature. For example, sample preparation units may be included upstream of the detection zone, for labeling, separation (e.g., magnetophoresis [4]) and positioning by hydrodynamic lateral, vertical, or even three-dimensional focusing [5–7] of the target analytes. Downstream of the detection zone, microfluidic structures for cell sorting may allow the separation and collection of the species of interest for further use in subsequent analysis giving rise to full sample-to-results devices (Fig. 2).

Despite several decades between the technological development of optical flow cytometry and MFC, and some recognized limitations of the technology, namely in the multiplexability potential to simultaneously measure different parameters on the same target entity, the area has generated great research activity as summarized in Table 2. Relevant advances regarding miniaturization, integration with fluidic and electronic components, sensor multiplexability, detection parallelization strategies, and fields of application are documented. The initial integration of spin valve sensors with microfluidic structures enabled the sensing of flowing ferrofluid droplets [17] and measurement of the flow velocities of magnetic particles [25]. Ferrofluid-based systems have been developed primarily as in-line, non-destructive detection methods to determine the magnetic properties of ultra-small volumes of magnetic nanoparticles (MNPs) in solution. Applications include quality control and basic understanding of magnetic phase formation during the synthesis and functionalization of superparamagnetic nanoparticles [12], and control synthesis and screening of magnetic suspension arrays [9], which are being investigated to expand the MNPs encoding capability. However, the applicability of ferrofluids in the biomedical field opens the potential to explore such systems as magnetic flow cytometers either for in vivo magnetic resonance imaging (MRI) [9] or as biomolecular tags for ex vivo biofluid analyses with lab-on-chip technology. Also, micron-sized and nanometric magnetic particles are widely explored either individually as proof-of-concepts or as labels of animal cells and bacteria in bioanalysis.

For multiplexing purposes, different types of encoded microcarriers, providing distinct magnetic signals, have been purified and identified into different batches (analogous to optical colored codes) by magnetic flow cytometric systems with integrated magnetic detectors [10]. In this context, magnetic labels of different materials,

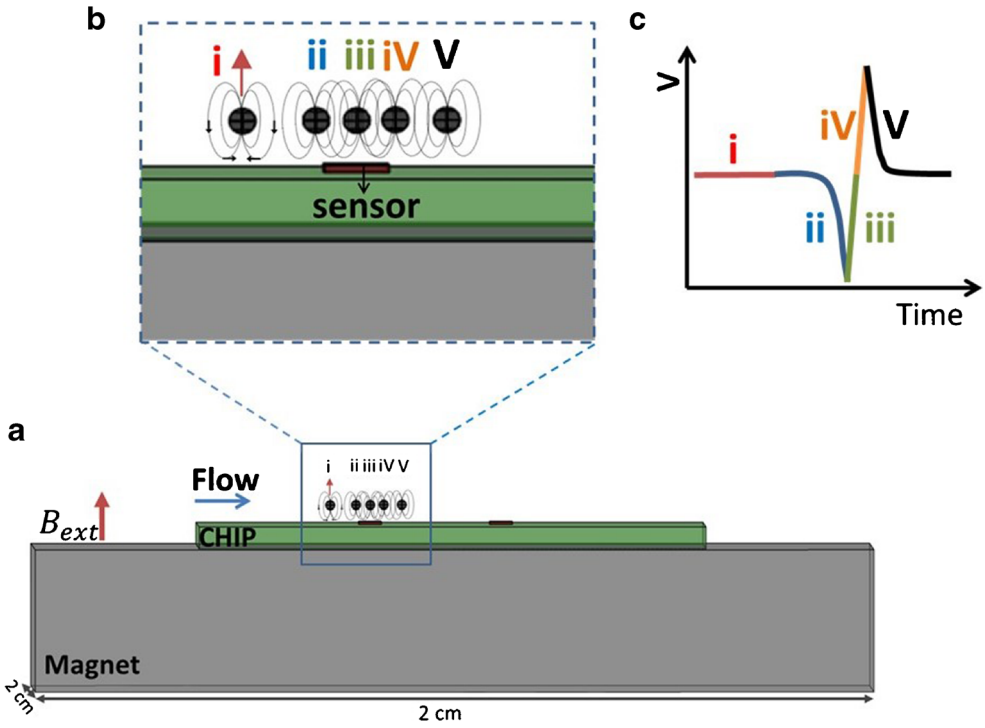

Fig. 1 Schematic representation of the MFC concept for magnetic particle detection. **a** A permanent magnet below the sensor is used for an out-of-plane magnetization of the superparamagnetic particle that flows inside a microfluidic channel. **b** Inset image of a particle passing over the sensor. **c** Signal output for a single particle for each one of the positions over the sensor

classified by the difference in their magnetic properties, are being explored to discriminate between different targets and parameters in the same target, similar to the colors of fluorescent labels [26, 31].

Table 1. Comparison of the gold standard optical flow cytometry and magnetic flow cytometry as techniques for cellular analysis

	Optical flow (OFC)	Magnetic flow (MFC)	Comments
Instrumentation complexity and expense	–	++	OFC: Expensive and complex optics MFC: Relatively inexpensive materials (e.g., thin-film chips and plastics), standard fabrication processes (semiconductor industry)
Size/portability	–	++	OFC: Bulky, benchtop size MFC: Potentially compact and portable for PoC usage
Sample preparation requirements	–	+++	OFC: Extensive protocols for sample preparation MFC: Besides magnetic labeling does not require any other sample preparation steps
Operator expertise	–	++	OFC: Need expert and trained personnel MFC: May integrate most functionalities in the device making it easy to operate
Number of parameters detected per analyte	+++	–	OFC: Up to 30 parameters MFC: Single parameter per analyte
Quantitation	+++	+++	OFC: Easily obtained statistics using embedded software MFC: Counts analytes at cm/s flow velocities
Sensitivity	+++	+++	OFC: Dependent on the fluorochromes, experimental design, and instrumentation MFC: Depends on the type of sensor, magnetic labels, experimental design, and instrumentation
Throughput	–	++	OFC: Analyze one sample at a time MFC: Can analyze several samples in parallel in microfluidic multichannel format (so far up to 6)
Cost of analysis	++	+++	OFC: Moderately expensive sample processing MFC: Avoids sample processing costs

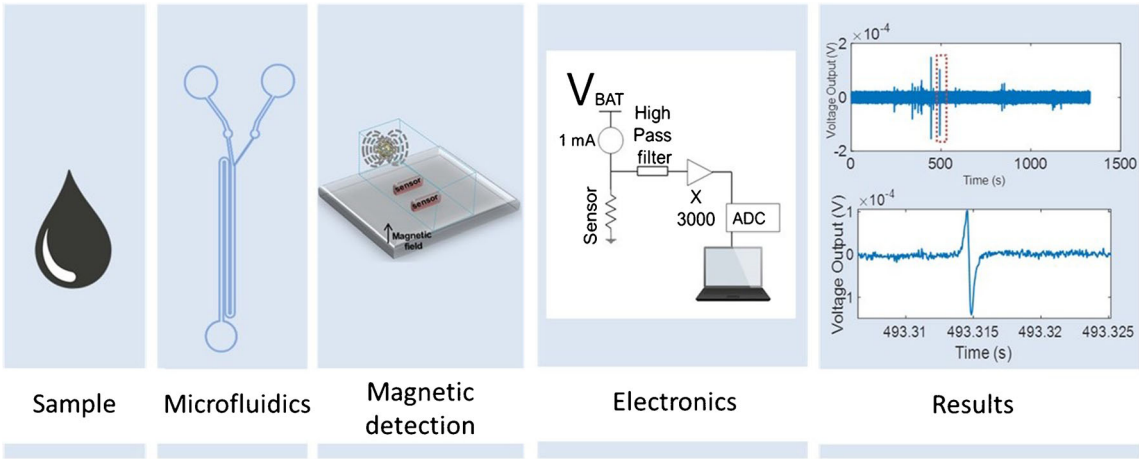

Fig. 2 Conceptual image of the different modules of a magnetic cytometry device

In this context, the present review covers the most recent developments and advances on MFC systems. New sensing architecture, multifunctional magnetic labels, and microfluidic designs that are being pushed for the analysis of complex biological samples, such as blood [24, 30] and milk [33], are discussed.

Emerging designs using ferrofluids and integration within flexible and stretchable substrates that further extend the scope of applications for MFC technology are also acknowledged.

Sensing technologies for magnetic cytometry

Table 2 shows the different types of magnetic field sensors that have been used for MFC. Those sensors are magnetic field transducers whose output voltage signal (V_s) is linearly proportional to an external applied magnetic field (H). This section provides a brief overview of the different types of sensors and physical characteristics will be described.

Magnetoresistive sensors

Among the magnetic field sensors used in MFC, magnetoresistive sensors have been the most ubiquitous and therefore will be analyzed in more detail. These sensors are characterized by the linear change of their electrical resistance with small magnetic fields and their response to an external magnetic field (transfer curve) can be of two types (Fig. 3). Sensors with transfer curves like Fig. 3a, such as planar Hall, spin valve, and magnetic tunnel junction sensors, typically exhibit the linear region centered at 0 T field. Thus, no external field is necessary to center the response of these sensors in the most sensitive region (i.e., linear zone). Transfer curves like in Fig. 3b typically show a resistance close to R_{max} at 0 T field; thus, it is necessary to apply an external magnetic field to obtain their maximum sensitivity.

The performance of these sensors is related to two characteristics: the magnetoresistance (MR) and the sensitivity (S). The MR (Eq. 1) corresponds to the maximum variation of the resistance while S is defined as the slope of the linear zone (Eq. 2).

$$\mathrm{MR} = \frac{R_{\max} - R_{\min}}{R_{\min}} \quad [\%] \tag{1}$$

$$S = \frac{1}{R_{\min}}\frac{\partial R}{\partial H} = \frac{1}{R_{\min}}\frac{\Delta R}{\Delta H} = \frac{\mathrm{MR}}{\Delta H} \quad [\%/\mathrm{T}] \tag{2}$$

where $R_{min}$is the minimum resistance, R_{max} is the maximum resistance and ΔH is the field span where the sensor is linear.

Three phenomena of magnetoresistance are known: anisotropic magnetoresistance (AMR) effect, giant magnetoresistance (GMR) effect, and tunneling magnetoresistance (TMR).

AMR

AMR sensors are based on spontaneous electrical resistance anisotropy observed in ferromagnetic materials (i.e., Ni, Co, Fe, and their alloys). The origin of this effect is attributed to a different scattering of electrons when the magnetization of the material is parallel or perpendicular to current [36]. For a measurement configuration as depicted in Fig. 4a, the magnetization of the ferromagnetic layer (typically NiFe) should be oriented parallel to the biasing current leading to a transfer curve similar to Fig. 3b. AMR sensors with MR up to 2% with soft permalloy films have been reported [37].

The planar Hall effect takes advantage of this anisotropy of the resistivity by measuring the Hall voltage on a cross measurement configuration (Fig. 4b) and are sensitive to in-plane fields [38]. To achieve a transfer curve similar to Fig. 3a, the magnetization of the ferromagnetic layer (typically NiFe) should be oriented parallel to the biasing current. This can be achieved by coupling an antiferromagnetic material (e.g., MnIr) to the sensing NiFe layer [39, 40]. For NiFe films

Table 2. Compilation of representative publications in magnetic flow cytometry

Sensor type	Sensor configuration	Microfluidic channel	Magnetic particles	Particles magnetization	Analytical sample	Key points	Reference
Ferrofluid nanoparticles							
Atomic magnetometer	Spin-exchange relaxation-free (SERF) optically pumped atomic magnetometer (OPAM) (QuSpin Inc)	Fresenius Heidelberger extension lines ∅ in = 3 mm ∅ out = 4.1 mm	C/Fe_3C ∅ = 24 nm; C/Co ∅ = 34 nm; Nanomag-D, Micromod ∅ = 130 nm	Pre-magnetization step Permanent magnet Halbach array system (ca. 2 T) Additional ring magnet	Nanoparticles in DI water and blood dispersions	In-line direct measurement of trace quantities of ferromagnetic nanoparticle Sensitivity, picomolar range	Bougas et al., 2018 [8]
GMI microwire	CoFeSiBNb alloy (MXT Inc) L = 10 mm ∅ = 40 μm	PDMS Y-shaped inlet junction W = 70 μm H = 170 μm L = 490 μm	USPIO, Guerbet ∅ = 20 nm	Pair of Helmholtz coils (1.9 kHz/8 mT)	Nanoparticles (230 mmol/L)	In-flow detection of ultra-small superparamagnetic particles Sensitivity, nanomolar range	Fodil et al., 2016 [9]
GMR multilayer	Wheatstone bridge (single) Meander shape with 9 turns of stripes Each stripe: W = 6 μm L = 100 μm	PDMS Two confronting T-junctions W = 100 μm H = 100 μm	FluidMAG, Chemicell GmbH ∅ = 50 nm	Permanent magnet (AlNiCo 500, type A1560, IBSMagnet) L = 60 mm ∅ = 15 mm	Nanoparticles in DI water (15 and 5 mg/mL)	A compact system for screening and quality control in the synthesis of encoded magnetic microparticles Discrimination efficiency, 100%	Lin et al., 2016 [10]
GMR multilayer	Wheatstone bridge (single) Meander shape with 19 turns of stripes W = 3 μm L = 100 μm Total sensing area ca. 100 × 100 μm^2	PDMS Two confronting T-junctions W = 100 μm H = 80 μm	FluidMAG-PAS, Chemicell GmbH ∅ = 50 nm	Permanent magnet (A1045, IBSMagnet) placed under the sensor	Nanoparticles in DI water (25 mg/mL)	Magnetic nanoparticles as joint barcodes to conventional optical encoding schemes Encoding capacity > 10 unique magnetic codes in addition to each optical barcode	Lin et al., 2015 [11]
Planar Hall effect	Cross-junction Active area 15 × 15 μm^2 Arm 400 μm	PDMS crossed-channel architecture W = 20 μm H = 25 μm	EFH1 (3–15% magnetite), Ferrotec, USA	Perpendicular Helmholtz coils ∅ in = 15 cm	Ferrofluid solution in oil (volume susceptibility of 7.54 emu/cc @ 100 Oe)	On-chip magnetometer with planar Hall sensors for online monitoring of small volumes of ferrofluids Sensitivity, μV/Oe range (35 pL droplet volume)	Kim et al., 2015 [12]
GMR multilayer	Wheatstone bridge (single) W = 6 μm L = 100 μm	PDMS W = 100 μm H = 100 μm	EMG 700, Ferrotec, USA ∅ = 10 nm	Permanent magnet placed below the sensor	Nanoparticles in DI water	Demonstration of the first flexible microfluidic analytic device with integrated GMR sensors LoD 2 × 10^{-10} emu (0.5 pL droplet volume)	Lin et al., 2014 [13]
GMI microwire	CoFeSiBNb alloy L = 1 cm ∅ = 40 μm	Glass	USPIO, Guerbet ∅ = 20 nm	Pair of Helmholtz coils in an AC magnetization field (1 kHz/ 9200 A/m)	Nanoparticles in fluid (18 mmol (Fe)/L)	New configuration of a GMI microwire sensor detection system for flowing magnetic nanoparticles Droplet volume 180 nL	Fodil et al., 2013 [14]
GMR multilayer	Wheatstone bridge (single)	PTFE tubing ∅ out = 0.9 mm	EMG 700, Ferrotec, USA	Permanent magnet (AlNiCo 500, type	Nanoparticles in fluid (75 mg/mL)	Magnetoresistive emulsion analyzer	Lin et al., 2013 [15]

Table 2. (continued)

Sensor type	Sensor configuration	Microfluidic channel	Magnetic particles	Particles magnetization	Analytical sample	Key points	Reference
	W = 1 mm L = 16 mm	∅ in = 0.4 mm	∅ = 10 nm	A1560, IBS Magnet) placed below the GMR sensor L = 60 mm ∅ = 15 mm		Magnetic-activated sorting of ferrofluid droplets Droplet volume 20–500 nL	
GMR multilayer	Sensor on a free-standing PDMS membrane L = 3.2 mm	Teflon tube ∅ in = 1.5 mm ∅ out = 3.2 mm	FeNdB magnetic particles (QJK-ES, FOB, Shanghai) 1 mm clusters	N.A.	Particles in mineral oil + 2% (v/v) sorbitan monooleate	Elastic and stretchable magnetic sensor around capillary tubing Sensitivity, isotropic	Melzer et al., 2012 [16]
Spin valves	Wheatstone bridge (half)—3 bridges W = 20 μm L = 34 μm	Two perpendicular channels Bottom channel: Cyclotene polymer W = 13 μm H = 18 μm Lid channel: PDMS W = 30 μm H = 25 μm	Ferrotec EMG 507 ∅ = 10 nm	Miniature electromagnet	Nanoparticles in water	Velocity and size monitoring of flowing ferrofluid droplets with GMR sensors	Pekas et al., 2004 [17]
Unconjugated magnetic particles							
Spin valves	Wheatstone bridge (half) W = 2 μm L = 30 μm	4 enrichment sections total length of ca. 29 cm	Micromer®-M, Micromod ∅ = 6 and 12 μm	NdFeB permanent magnet (IBSmagnet) 75 × 50 × 10 mm^3 Underneath the channel	Microparticles in whole blood	Scalable particle focusing concept, combining mechanical and magnetophoresis with time-of-flight approach Miniaturization of the Si footprint for bedside testing	Reisbeck et al., 2018 [18]
Spin valves	6 groups of 4 sensors W = 3 μm L = 200 μm	PDMS 6 individual channels W = 300 μm H = 50 μm	Dynabeads MyOne streptavidin T1 and M-280, Invitrogen ∅ = 1 and 2.8 μm	Customized permanent magnet W = 35 mm H = 9.7 mm out-of-plane magnetic field (> 100 mT)	Microparticles in PBS solution + 0.5% BSA (1000 and 5000 beads/μL)	Multiple microchannels; custom-made PM with high out-of-plane magnetic field (> 100 mT) and low transverse in-plane field (< 1 mT)	Chícharo et al., 2018 [19]
GMI	Planar samples FeCoCrSiB amorphous ribbons H = 21 μm W = 1 mm Permalloy-based sputtered trilayer with a special structure	COC chamber (10 μL) connected to 2 channels	Ferromagnetic SiMAG/MP-DNA, Chemicell GmbH Silica shell ∅ = 2 μm Dynabeads M-450, Invitrogen ∅ = 4.5 μm	Pair of Helmholtz coils	Microparticle suspension in phosphate buffer saline (PBS)	GMI sensor for the detection of magnetic beads under continuous flow	García-Arribas et al., 2011 [20]
GMR multilayer	Wheatstone bridge (half) Meander with 2.5 to 8.5 periods W = 4 μm	Rolled-up tube with GMR L = 15 mm ∅ = 60 μm	CrO_2 nanoparticles, Magtrieve, encapsulated into a polymeric hydrogel shell (8 wt% of CrO_2)	Electromagnet (80 mT)	Microparticles in organic solvent (toluol)	Fully integrative rolled-up GMR acting as a fluidic channel for in-flow detection of magnetic particles	Mönch et al., 2011 [21]

Table 2. (continued)

Sensor type	Sensor configuration	Microfluidic channel	Magnetic particles	Particles magnetization	Analytical sample	Key points	Reference
	L = 200 μm Active sensors rolled-up into a tubular geometry, reference sensors in planar		∅ = 40 ± 10 μm			No need for an external magnet Sensitivity, differential sensitivity to weak magnetic fields (2.8 mV/mT at ca. 1.4 mT)	
Hall effect	InAs quantum well array of 6 Hall crosses $A = 1 \times 1\ \mu m^2$	PDMS W = 1000 μm H = 200 μm	SPM beads, Bangs Laboratories, Inc. ∅ = 2.6 μm	AC field 0.9 mT/93 Hz DC field (70.6 mT)	Microparticles in DI water	First integration of InAs micro-Hall sensors with microfluidic channels and real-time detection of micron-sized SPM beads	Aledealat et al., 2010 [22]
Spin valves	Array of 4 sensors W = 2.5 μm L = 40 μm	PDMS W = 150 μm H = 14 μm	Micromer-M, Micromod ∅ = 2 μm	Permanent magnet below the PCB	Microparticles in phosphate buffer	Determination of the magnetic orientation, flowing height, and speed of single magnetic beads	Loureiro et al., 2009 [23]
Spin valves	Array of 3 sensors yoke shape geometry W = 2.5 μm L = 40 μm	PDMS two parallel micro-channels H-shaped W = 150 μm H = 14 μm	Micromer-M, Micromod ∅ = 2 μm	Permanent magnet under the chip (90 mT)	Microparticles in phosphate buffer	Detect single magnetic bead motion (speed, flowing height, magnetic orientation) at cm/s velocities	Loureiro et al., 2009 [4]
MTJs	Elliptical W = 2 μm L = 6 μm	PDMS W = 600 μm H = 50 μm	Dynabeads® M-280 ∅ = 2.8 μm	Two crossed pairs of toroidal electromagnets, in-plane static magnetic fields	Microparticles in DI water	Real-time detection of moving individual micron-sized magnetic beads SNR 16	Shen et al., 2005 [24]
Spin valves	Pair of sensors separated by 1.65 mm W = 2 μm L = 6 μm	PDMS W = 100 μm H = 20 μm L = 2.8 mm	Nanomag-D, Micromod ∅ = 250 nm	Planar electromagnet $Ni_{80}Fe_{20}$ circular core positioned over the chip carrier (ca. 15 Oe)	Particles in water or buffer	Measurement of magnetic particles flow velocities on microfluidic devices	Ferreira et al., 2004 [25]
Magnetically labeled eukaryotic cells							
Spin valves	6 groups of 4 sensors W = 3 μm L = 220 μm	PDMS 6 individual channels W = 300 μm H = 50 μm	Masterbeads Streptavidin Ademtech ∅ = 500 nm	Custom-made permanent magnet toroid shape placed below the PCB (100 mT)	Labeled SW480 cells derived from colon adenocarcinoma in buffer	Signal improvement of 246% with 3D hydrodynamic focusing system SNR 50	Chícharo et al., 2018 [5]
Inductive	Symmetric 6 turn spiral on top of 2 metal layers	PDMS W = 200 μm H = 100 μm	Validation: Dynabeads ∅ = 4.5 μm Tests: $MnFe_2O_4$ OceanNanotech Inc. ∅ = 800 nm–1 μm	Weak magnet beneath the CMOS chip (10 mT)	Labeled cells in buffer	Classification of magnetic labels made of different materials by the difference in the phase of their complex susceptibility SNR 11 dB	Murali et al., 2017 [26]
Spin valves	Wheatstone bridge (half) W = 2 μm L = 30 μm	Cross section W = 700 μm H = 150 μm L = 15 mm	Validation: Micromer-M, micromod, GmbH ∅ = 12 μm Tests: anti-CD235a functionalized MNPs,	NdFeB permanent magnet placed underneath the sensor $32 \times 27 \times 5\ mm^3$ (100–170 mT)	Whole blood with nanoparticles in buffer	Highly deterministic cell focusing approach (fluidic + magnetophoretic forces)	Reisbeck et al., 2016 [27]

Table 2. (continued)

Sensor type	Sensor configuration	Microfluidic channel	Magnetic particles	Particles magnetization	Analytical sample	Key points	Reference
			MACS MicroBeads, Miltenyi Biotec GmbH			Time-of-flight (TOF) approach to determine cell morphology based on the magnetic fingerprint	
Spin valves	Wheatstone bridge (single) GMR discs: ∅ 150 μm	PDMS W = 60 μm H = 47 μm L = 250 μm	Ferrotec EMG 705 ∅ = 10 nm	Coil under the cell counter	Mouse monocyte-macrophage cells and nasopharyngeal carcinoma cells with magnetic particles inside	Cell sorting of particles with different magnetic moments using magnetic field gradients for the separation of cells into different channels	Lee et al., 2014 [28]
Spin valve	W = 3 μm L = 20 μm	PDMS W = 200 μm H = 100 μm	Polymeric beads loaded with magnetite nanoparticles ∅ = 120–200 nm	Permanent magnet under the PCB Vertical direction	EpCAM cancer cells labeled with nanoparticles in buffer	Tailoring of magnetic beads to be used as magnetic labels for magnetic flow cytometer	Vila et al., 2014 [29]
Inductive	2 coils connected in series with opposite polarity Coil size 30 × 30 μm Coil gap 12 μm	PDMS W = 200 μm H = 50 μm	Dynabeads Streptavidin ∅ = 4.5 μm	Polarization B-field generated by an on-chip coil surrounding the pickup (GHz range)	mEFs cells labeled with microparticles in buffer	Monolithic integration in standard CMOS process Differentiation of magnetic bead based on ferromagnetic resonance Throughput 20 cells/s	Boser and Murali, 2014 [30]
Spin valves	Wheatstone bridge (half: diagonal vs parallel geometry) W = 2 μm L = 30 μm	PDMS W = 700 μm H = 200 μm	SPION ∅ = 12 nm	Permanent magnet underneath the microfluidic channel (200 mT)	Labelled FaDu cells in EDTA whole blood (non-hemolyzed)	TOF measurement to detect specifically cancer cells and cells' diameter in whole blood Magnetophoretic enrichment and focusing Throughput 10 cells/s	Helou et al., 2013 [18]
Micro-Hall sensors	Array of 8 sensors 8 × 8 μm^2	PDMS	Tetrazine (Tz)-modified microparticles ∅ = 3 and 8 μm	Neodymium permanent magnet below the chip (ca. 1 cm^3) (ca. 0.5 T)	Labeled cancer cell lines in whole blood	Measure single cells in whole blood Simultaneous detection of two biomarkers in individual cells Throughput 10^7 cells/min	Issadore et al., 2012 [31]
Spin valves	Array of 3 sensors W = 3 μm L = 40 μm	PDMS W = 150 μm H = 14 μm	CD34 microbeads, Milteny ∅ = 50 nm	Permanent magnet below the chip/PCB (190 mT)	Labeled KG1-a cells in PBS	Real-time detection of single magnetically labeled cells with speeds around 1 cm/s	Loureiro et al., 2011 [32]

Table 2. (continued)

Sensor type	Sensor configuration	Microfluidic channel	Magnetic particles	Particles magnetization	Analytical sample	Key points	Reference
Magnetically labeled bacteria cells							
Spin valves	Array of 7 sensors in a line $W = 3$ µm $L = 100$ µm	PDMS $L = 100$ µm $H = 50$ µm	Nanomag®-D-spio Protein A $\varnothing = 50$ nm	Permanent magnet below the PCB, (NdFeB, Supermagnete)	Labeled *Streptococci* in PBS and milk samples	Real mastitic milk sample analysis LoD 100 cfu/mL Accuracy 73% for *Streptococci* species	Duarte et al., 2016 [33]
Spin valves	4 sets of 7 sensors disposed in a line $W = 3$ µm $L = 20$ to 100 µm	PDMS 4 parallel channels $H = 100$ µm $W = 100$ µm $L = 1$ cm	Nanomag®-D-spio Protein A $\varnothing = 50$ nm	Permanent magnet below the PCB (NdFeB, Supermagnete) $20 \times 20 \times 3$ mm^3	Labeled *Streptococcus agalactiae* in defatted milk	Identification and counting of bacterial cells in milk Multiple channels for multiplexing	Fernandes et al., 2014 [34]
Micro-Hall sensors	8 sensors in overlapping 2×4 array 8×8 µm^2	PDMS $W = 200$ µm $H = 15$ µm	Cross-linked dextran iron oxide nanoparticles functionalized with tetrazine (Tz)	Neodymium permanent magnet below the chip (ca. 1 cm^3) (ca. 0.5 T)	Labeled Gram+ and Gram− bacteria in liquid media	Microfluidic chip-based and minimal sample processing LoD 10 bacteria	Issadore et al., 2013 [35]

ranging from 20 to 30 nm, a relative resistance variation $\frac{\Delta\rho}{\rho_\perp}$ in the order of 2–3% was measured [39–41].

GMR

The GMR effect, first discovered by Albert Fert [42] and Peter Grünberg [43], relies on spin-dependent transmission of conduction electrons between two ferromagnetic (FM) layers through a metallic layer (M). A GMR device is typically composed of one or more repetitions of the multilayer stack FM1/M/FM2. In this device, the electrical transport can be divided into two spin channels, namely the spin-up and spin-down channel. The FM layers can be in a parallel (Fig. 5a) or antiparallel (Fig. 5b) configuration. In the first case, spin-down electrons will have a higher scattering probability than the spin-up electrons. This creates a lower resistivity channel for spin-up electrons which lowers the overall resistance of the device (Fig. 5a). In the second case, spin-up and spin-down electrons will both have a high scattering probability in the respective FM layer with opposite moment generating two channels with the same resistivity (Fig. 5b). The resistivity of this channel is higher than the low resistance channel of the first case, therefore producing an overall higher resistivity than the parallel state.

A GMR stack is typically composed of several layers FM1/M/FM2 and has a magnetic response as depicted in Fig. 3b. The MR of these sensors can amount to 10%.

In 1991 Dieny et al. [44] introduced the principle of a spin valve sensor comprising a fixed FM layer (pinned layer) and an FM layer free to rotate with the external field. This concept was further developed and tested in 1994 [45]. The FM magnetic moment is typically fixed by coupling one of the FM layers to an antiferromagnetic layer such as MnIr, MnPt, MnNi, or MnFe. The spin valve configuration leads to a transfer curve as depicted in Fig. 3a. MR up to 20% were reported for spin valves [46].

TMR

The operation of TMR sensors is described by the spin-dependent tunneling effect. In this phenomenon, electrons tunnel across an insulating barrier (I) between two FM electrodes. The device composed of FM1/I/FM2, where FM2 is further pinned using an antiferromagnetic layer, is called a magnetic tunnel junction. For a sufficiently thin insulating layer, applying a voltage across the electrodes, the electrons will be able to tunnel through the insulator [46]. When the magnetizations of the FM layers are in a parallel (antiparallel) state, a low (high) electrical resistance will be measured at the sensor terminal. It was demonstrated that MTJ can attain an MR up to ca. 500% at room temperature [47].

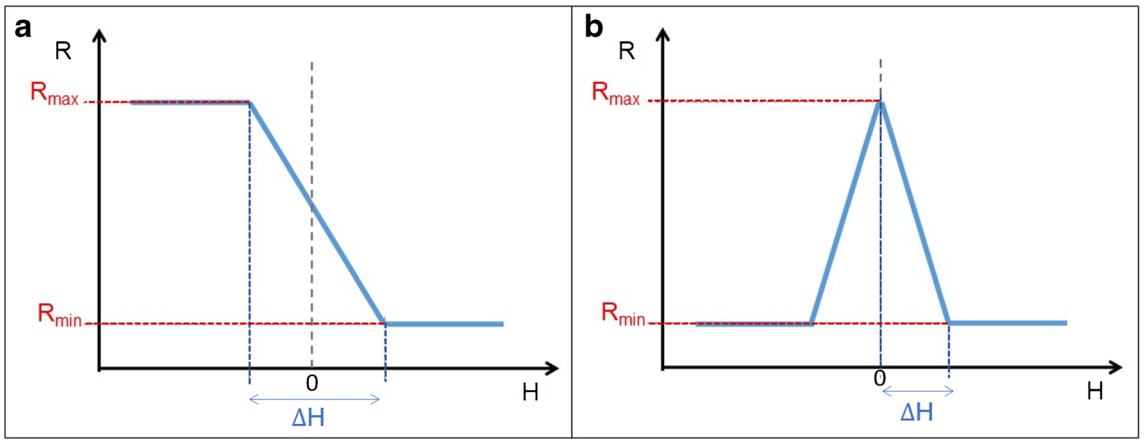

Fig. 3 Schematic representation of linear magnetoresistive sensors transfer curves for **a** spin valves, magnetic tunnel junctions, and planar Hall; **b** AMR and GMR multilayers

Comparison of MR sensors

Table 3 shows expected signal-to-noise ratio (SNR) depending on the MR sensor type. For MFC applications, in general, sensors measure the average fringe field of the magnetic entities over the sensing area. To allow a fair comparison, sensors with similar area were chosen to remove any geometrical signal enhancement.

GMR stack and spin valve are the sensors with the lower expected SNR since they are the ones with lower sensitivity. Their noise is also higher than the PHE sensors but not higher than MTJs. The sensitivity of MTJs is maximized when voltages below ca. 50 mV are applied. However, their large MR, yielding a ratio $\frac{R_{\min}}{R_{dc}} = \frac{2}{3}$, attenuates the SNR. Also, MTJs show higher noise when compared to the PHE sensors. On the other hand, when choosing a type of sensor, besides their intrinsic noise, it is also important to analyze the contribution from the signal acquisition system. While the higher noise exhibited by MTJs can be a downside for this type of sensor, the challenge to design electronic systems with noise specification lower than PHE sensor noise cannot be overlooked. Most of the time, the limiting noise arises from the acquisition system, degrading in this way the total SNR. In this context, although presenting higher noise, MTJ sensors may be of a great advantage since the noise added by the acquisition system will be negligible. In this particular case, MTJ has higher SNR of all MR sensors. If a very low noise acquisition system can be designed, the PHE sensor will be the one exhibiting higher SNR.

Other magnetic sensors

Besides MR sensors, other magnetic field sensors have been also used: Hall effect, inductors, GMI, and atomic magnetometers.

Hall effect sensors rely on the measurement of the voltage (V_H) perpendicular to the current passing through a conductor caused by the deflection of the electrons due to an out-of-plane magnetic field. These sensors have typical sensitivities up to

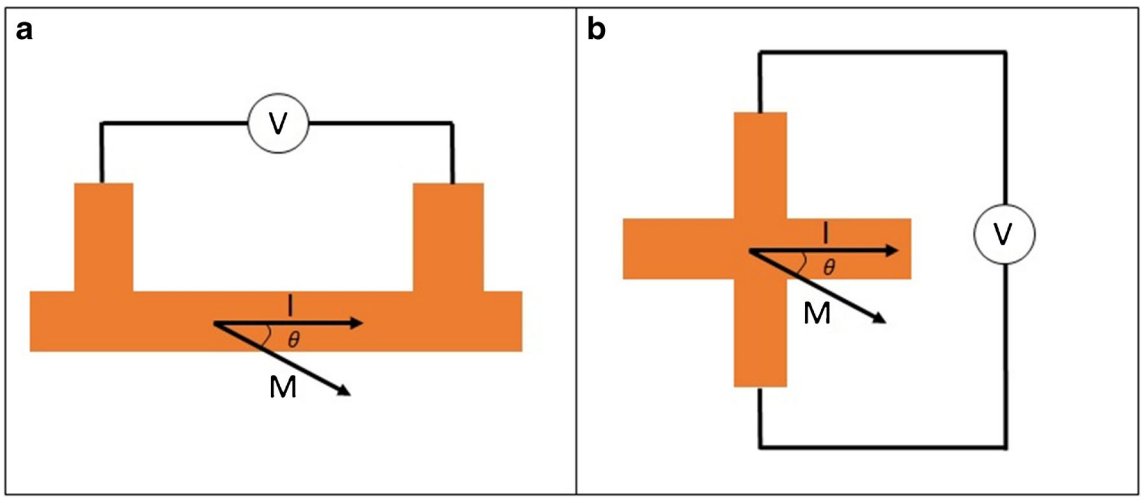

Fig. 4 Typical measurement configurations for **a** AMR and **b** planar Hall

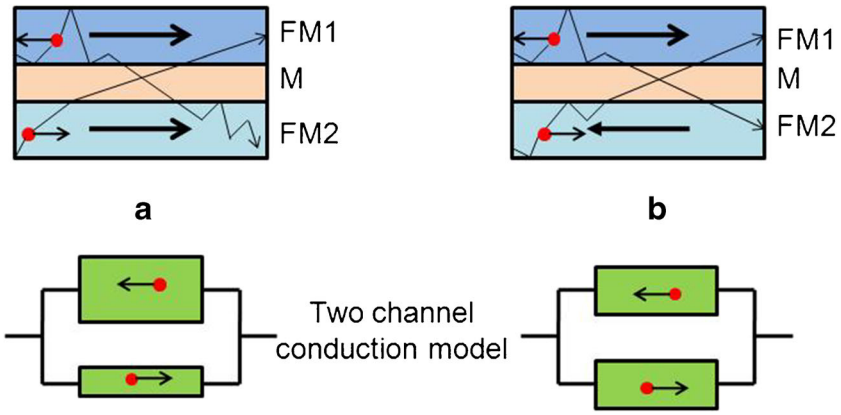

Fig. 5 Schematic of the GMR effect in FM1/M/FM2 structure when FM1 and FM2 are **a** parallel or **b** antiparallel. The two-channel conduction model is illustrated. In this model, each spin channel is represented by a resistor. If the spin of the electron has the same orientation as the moment of the layers, the resistance is low. In the opposite case, the resistance is high. The overall device resistance is the parallel equivalent of the resistance of both spin channels

175 V/(T.A) [30, 41], linear response over a large range of field but present higher noise than MR sensors. Inductors rely on Faraday's law. Briefly, a voltage is generated in a coil upon application of an out-of-plane alternating magnetic flux. The sensitivity of inductors increases with the frequency, and therefore large frequencies (gigahertz range) are typically used to measure small magnetic flux as is the case for MFC [26]. GMI sensors resort to the skin-depth effect which creates a change in the sensor impedance as an AC current flows inside an electrical conductor. This impedance varies with the inverse of the square root of the frequency and of the magnetic permeability. A change in the external magnetic field will cause a variation of the magnetic permeability of the material and therefore the impedance of the sensors. These sensors typically operate at tens of megahertz and can detect fields down to a few nanotesla [14]. Finally, atomic magnetometers are devices made up of atomic gases (rubidium or cesium) and use the Zeeman effect. This is a quantum effect where the magnetic spin of atoms changes with an external magnetic field. A pump laser is used to set the atoms to a specific spin state while a probe laser measures the spin state of the atoms which varies with the external magnetic field. This is the most sensitive magnetometer at room temperature, although complex apparatus including two lasers and a shielded box is required [8].

Magnetic detection system

Magnetic labels

Labeling considerations

The biological entities targeted in this type of detection system are non-magnetic in nature and thus invisible to the magnetic sensors in use. Therefore, magnetic particles are required to mark the targets and work as reporter systems.

Magnetic labels and their respective magnetic moments contribute to define the sensitivity and accuracy of the assay, as well as the assay specificity determined by their surface functionalization. Therefore, cautious selection of the magnetic particles must be undertaken considering their magnetic,

Table 3 MR sensors SNR comparison

Type of sensor	Area (μm^2)	Sensitivity (mT^{-1})	Hooge constant	SNR ($\sqrt{Hz}/mT$)	Reference
PHE	225	0.317	0.01	1.69×10^7	[10]
GMR stack	300	0.03	1	8.87×10^5	[12]
Spin valves	300	0.024	0.1	1.27×10^6	[34]
MTJ	300	0.2	1×10^9 μm^2	5.16×10^6	–

The SNR for low frequencies were calculated using the equation $\mathrm{SNR} = \frac{S}{R_{dc}} R_{min} \sqrt{\frac{N_c f}{\alpha_H}}$ for PHE, GMR, and spin valve sensors, and $\mathrm{SNR} = S \frac{R_{min}}{R_{dc}} \sqrt{\frac{A f}{\alpha_H}}$ for MTJ sensors. R_{dc} is the sensor DC resistance (in most cases R_{dc} is the resistance at $H = 0$ Oe), N_c is the number of carriers on the conductive materials, α_H is the Hooge constant, A is the area of the sensor, and S is the sensor sensitivity. The frequency was assumed to be 5 kHz. The sensitivity and area were obtained in the references except for the MTJ sensor for which typical values were used. N_c were calculated on the basis of the sensor area and stack. Typical values of the Hooge constant were used for all the sensors. Finally, $\frac{R_{min}}{R_{dc}} = 1$ was assumed for PHE, GMR, and SV because of their low MR (< 10%). For MTJ sensor, an MR = 100% and a centered transfer curve were assumed, leading to $\frac{R_{min}}{R_{dc}} = \frac{2}{3}$.

physical, and biochemical characteristics together with the characteristics of the detection system and the envisioned application.

The magnetic properties of the particles are undoubtedly key features to consider. Particles can be superparamagnetic, i.e., non-remnant, because the magnetic material within the label exists as small particles (usually iron oxide), with small random moments. The detection system relies on the alignment of these moments when a magnetic external field is applied, generating a measurable fringe field.

Some attempts to discriminate between a panel of magnetic particles and use them for multiplexing purposes could be obtained using particles with different magnetization values [31] or different complex susceptibility at a given frequency of operation [26].

Regarding the physical characteristics of magnetic labels, size is the most relevant feature and is intimately related to the type of target entity, including (i) nature (i.e., if it is eukaryotic or a bacteria cell, spore (Fig. 6), or virus); (ii) size and surface area; (iii) available labeling sites, such as antibody-binding epitopes or other specific ligand recognition zones. Micrometric labels (up to 12 μm diameter) have been widely used in preliminary proof-of-concept experiments, using different types of sensors [4, 18–25]. They are easily observed under standard optical microscopes and are generally uniform in size and magnetic content. Although having a lower percentage of magnetic composition (ca. 15 wt%), in comparison to MNPs, their increased volume results in a higher magnetic moment per label. Thus, when submitted to an external magnetic field, detection of independent signals at the single label level is possible [48]. On the other hand, this may hamper the discrimination of free labels from labeled entities. Additionally, their higher density makes them behave differently from cells in microfluidic channels. They tend to sediment in the channels, and often accumulate in transition zones (e.g., inlets and outlets).

The most used magnetic nano-sized particles in biomedical in vivo applications are composed of the iron oxides magnetite (Fe_3O_4) and maghemite (γ-Fe_2O_3), and usually have a diameter range of 1–100 nm [3]. These smaller labels with a high magnetic content (70–85 wt%) are a better solution for labeling purposes in MFC applications, mainly because their smaller size allows higher labeling densities. However, they may suffer from higher dispersion in size and shape and their high magnetization and anisotropy for their volume, under an applied magnetic field, may lead to particle clustering. This can interfere with the detection of labeled entities, triggering false positive counts.

Although there is no "tried and true" way yet to address this issue, possible strategies are filtering the free MNPs and clusters from solution [49, 50], using microfluidics system architecture to separate unwanted nanoparticles, thus preventing them from reaching the proximity of the sensor, or taking advantage of magnetophoretic forces [51].

Vila et al. [29] have addressed this matter through the design and tailored production of polymeric nanobeads. The beads (∅ 120–190 nm) were loaded with different contents of magnetite nanoparticles ranging from 14 to 44 wt%. A fine tuning of the magnetic content of the beads allows the discrimination of free beads from labeled cells in a mixture flowing over the magnetic sensors. However, smaller labels of lower

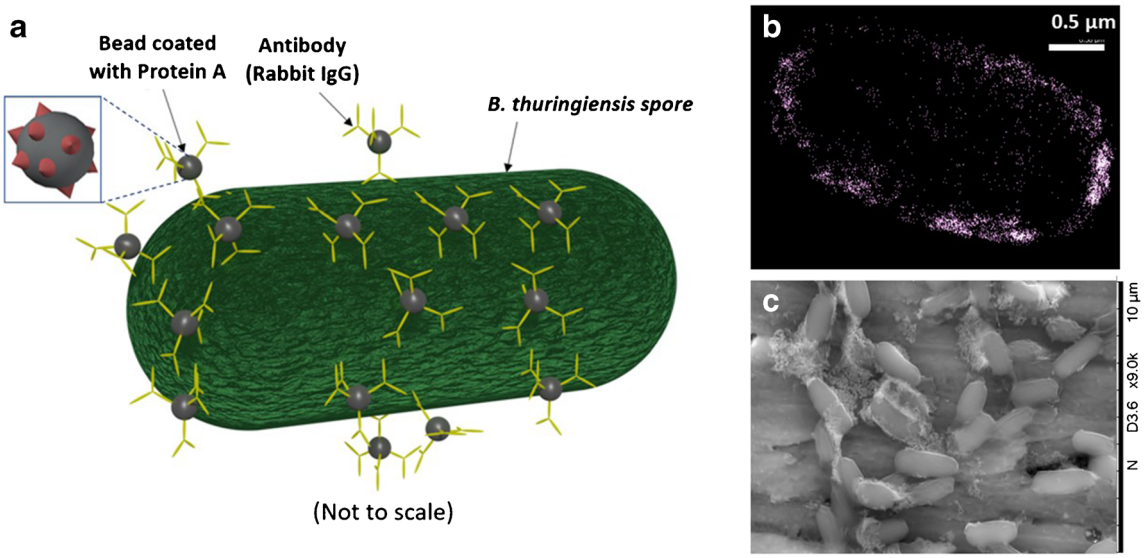

Fig. 6 **a** Schematic of a bacterial spore labeled with immunomagnetic nanoparticles. **b** STORM (Stochastic Optical Reconstruction Microscopy) image (× 50,000 magnification); Immunofluorescence image from *Bacillus cereus* reacted with rabbit anti-*B. cereus* antibody and goat anti-rabbit secondary antibody labeled with Alexa 647, presenting high labeling efficiency. **c** SEM picture of *B. thuringiensis* spores labeled with magnetic nanoparticles, presenting low labeling efficiency (× 20,000 magnification)

magnetic moment demand higher labeling densities of the target (more particles per target).

The most common way to label cells is the attachment of particles on their outer surface through a ligand molecule that makes the bridge between the magnetic particle and the cell (Fig. 6a). Such ligands are intended to be specific to particular sites, molecules, or epitopes in the cell surface. With the ever-growing area of biosensors, many types of novel ligands have been investigated and made available, including DNA aptamers, bacteriophages, and antibody fragments, among many others, from naturally occurring to synthetic origin. Antibodies are still the most commonly used for both standard flow cytometry and MFC.

Antibodies against specific biomarkers, like cell surface protein antigens (e.g., EpCAM), in the target cells are widely commercially available. They can be found unconjugated, modified with affinity molecules for further immobilization in the magnetic particle carrying the complementary ligand, or as labeling kits, consisting of magnetic particles pre-functionalized with specific antibodies. When working with unconjugated antibodies, one can use several functionalization chemistries to immobilize them to the magnetic markers. Some examples are (a) covalent chemistry, making use of the antibodies' native functional groups (e.g., amine, carboxylic, thiol, or aldehydes in the carbohydrate chain) to bind to the particle's surface through bifunctional linkers (e.g., glutaraldehyde, EDC/NHS, sulfo-EMCS, sulfo-SPDP); affinity reactions between an antibody's F_c region and protein A or G molecules on the particle's surface; biotinylation of the antibody and binding via biotin–streptavidin affinity reaction. These strategies are discussed in depth by Martins et al. [52]. Besides the decoration of the cell surface with magnetic labels, a less explored labeling alternative is the introduction of MNPs into the cells by endocytosis [28].

The type of sample, in particular complex biological fluids, is another critical aspect to think of when designing an MFC system. Viscous samples, such as blood and milk which were addressed in some of the reports, impose great challenges that can be tackled using sample preparation units integrated in the microfluidic systems. Magnetic separation strategies have been thoroughly explored as a purification and concentration approach, being an advantageous alternative [53].

Metallic ferromagnetic nanoparticles are particularly interesting for separation processes in complex media because they exhibit higher saturation magnetizations and allow for fast and complete separation using high gradient magnetic separators. For these reasons, they are being explored for many biomedical and industrial applications. For example for the monitoring of in vivo MRI particles and biomolecules tags for ex vivo biofluid analyses [8, 9]; and in quality control in the synthesis of encoded microparticles or water source remediation [10, 12]. Thus, ferromagnetic nanoparticles have been used as ferrofluids in MFC studies to demonstrate the potential of these systems to work for in-line direct analysis of such particles.

As stated previously, choosing the size of the magnetic label is intimately related to the nature of the intended target. Microbial cells are, on average, 10-fold smaller than mammalian cells (approximately 1 μm vs. 10 μm) and consequently have lower levels of many cell constituents, including surface antigens for magnetic labeling (Fig. 6b). These biological differences have great impact on the practical aspects of labeling (Fig. 6c). This aspect may explain the lower number of MFC works applied to the detection of bacteria [33–35].

Magnetic labels magnetization

As mentioned above, typically employed magnetic labels are superparamagnetic, do not express hysteretic magnetization curves, and have zero remanence. This means that these particles require an external source of magnetic field to induce a magnetic moment on them for magnetic detection purposes. In this respect, a magnetic particle can be approximated to a magnetic dipole and the stray field is given by Eq. 3:

$$\boldsymbol{B}(\boldsymbol{m},\boldsymbol{r}) = \frac{\mu_0}{4\pi}\left[\frac{3\boldsymbol{r}(\boldsymbol{m}.\boldsymbol{r})}{\boldsymbol{r}^5} - \frac{\boldsymbol{m}}{\boldsymbol{r}^3}\right] \tag{3}$$

where $\boldsymbol{B}(\boldsymbol{m},\boldsymbol{r})$ is the magnetic stray field, $\boldsymbol{m}$ is the magnetic moment at a vector distance $\boldsymbol{r}$, and μ_0 is the magnetic permeability.

Two main magnetic field generation strategies are used: permanent magnets and electromagnets. An important difference between these two strategies is the much lower magnetic induction generated by the electromagnet. A permanent magnet easily generates a magnetic induction of 0.5–1 T, while the electromagnet is typically in the millitesla range. An advantage of electromagnetic coils is that they offer flexibility, as the magnetic field can be simply switched off by setting the coil current to zero. However, they are usually bulky, have high power consumption and heating effects, hampering their application in PoC solutions.

The magnetic field can be applied in the plane or perpendicular to the sensor. According to the configuration and type of sensor, different pulse shapes will be measured. For MR sensors and an in-plane magnetization, the average fringe field has a unipolar configuration while the perpendicular magnetization affords a bipolar configuration (Fig. 7). In the in-plane configuration, it is important to avoid sensor saturation by applying a relatively low magnetic field. Larger out-of-plane magnetic fields (up 1 T) can be applied since this type of sensor is not sensitive to the field direction. Other types of sensors such as Hall effect sensors are sensitive to the out-of-plane field and therefore measure opposite pulse shapes to MR sensors.

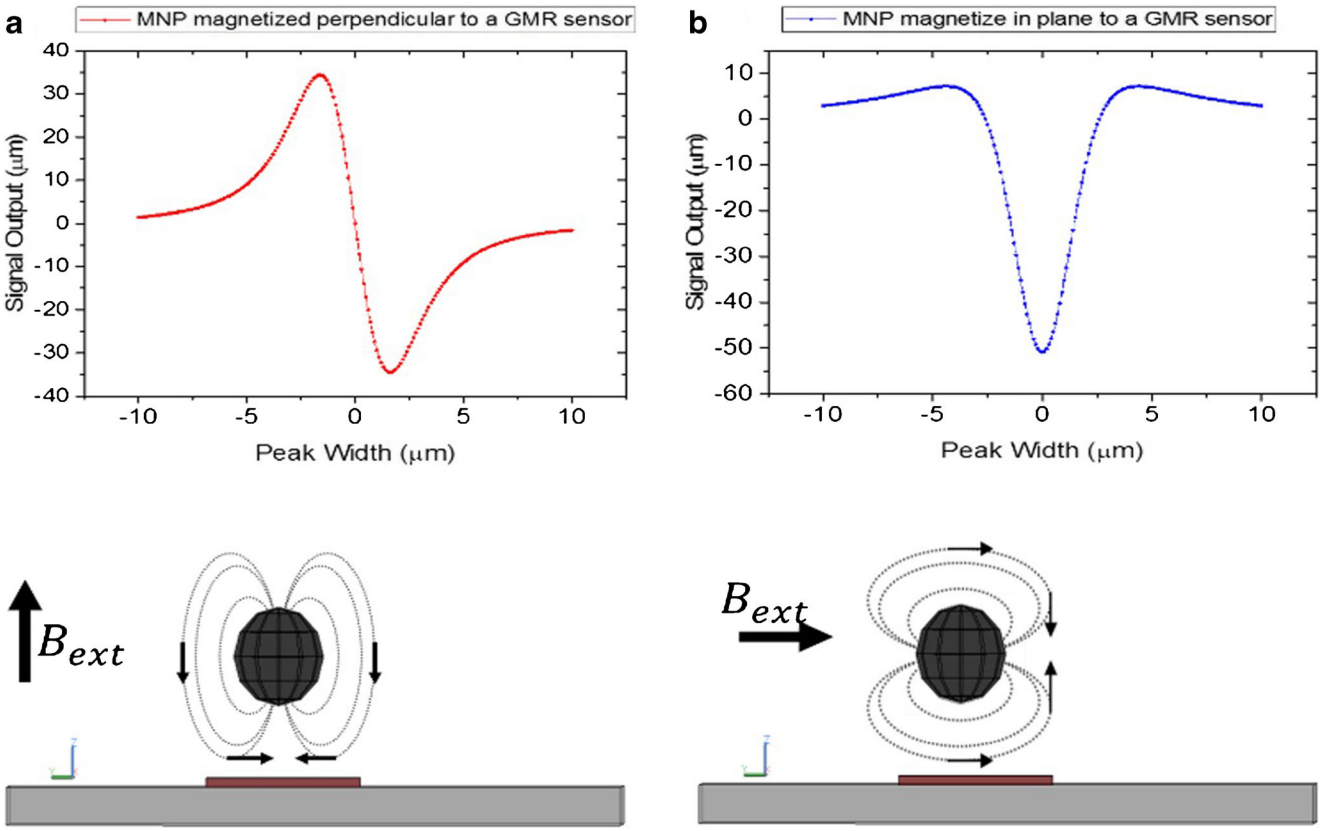

Fig. 7 Schematic representation of the signal output for an MR sensor when applying **a** perpendicular or **b** in-plane excitation field for a particle of 2.8 μm diameter (Dynabeads M-280 streptavidin) at 0.2 μm from the sensor

Commercial permanent magnets (e.g., AlNiCo 500 and NdFeB, IBS Magnet; NdFeB, Supermagnete) have been extensively used and are usually positioned under the chip for an out-of-plane magnetization of the labels. However, they require careful alignment with the sensing elements, because a small tilting of the magnet can create magnetic field components in the sensor plane which have a negative impact on their sensitivity (Fig. 8) [34]. By combining the scanning of the magnet positioning with transfer curve measurements it is possible to find the optimal site for maximum sensor output

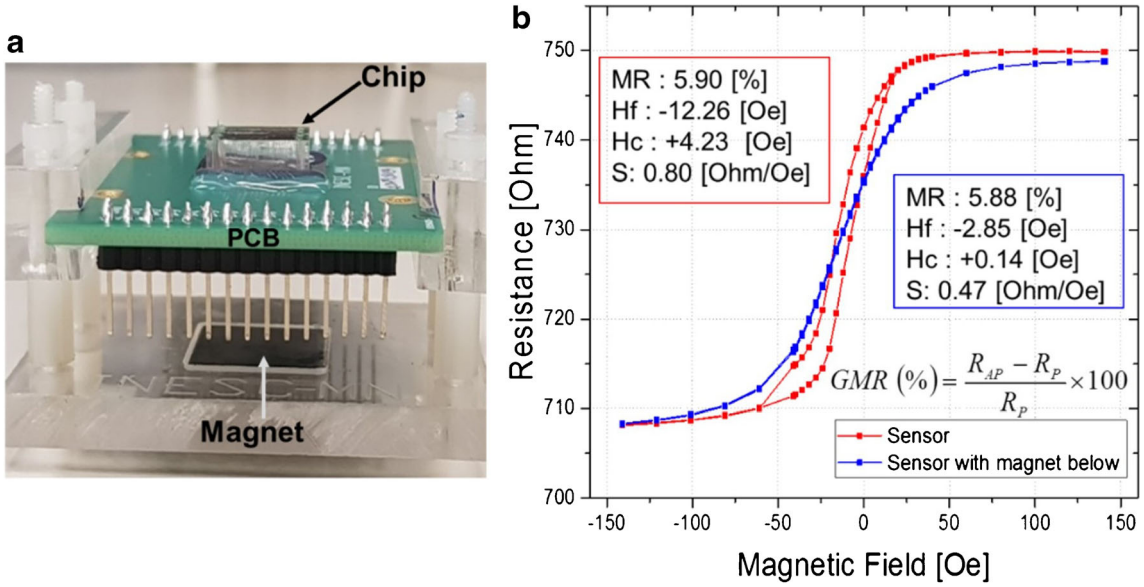

Fig. 8 **a** Integrated device comprising the chip and a microfluidic module in a PCB. A permanent magnet is placed below the chip for an out-of-plane particle magnetization. **b** Effect of a permanent magnet placed under the chip on the transfer curve of a spin valve magnetic sensor

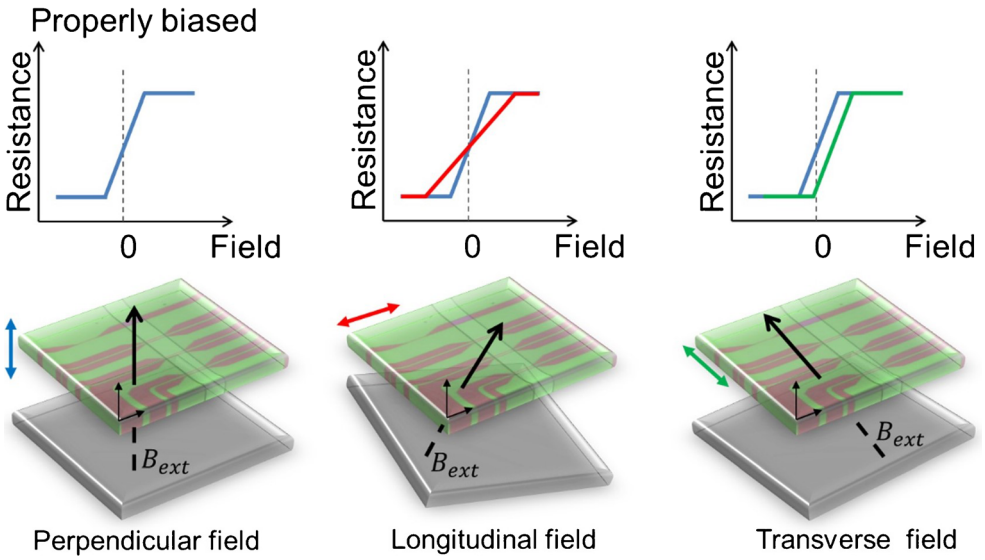

Fig. 9 Schematics illustrating the impact of the permanent magnet positioning in the sensor's response. A tilt of the magnet creates fields in the sensor plane, shifting the sensor transfer curves and decreasing the sensor sensitivity

(Fig. 9). However, the magnetic field coming from permanent magnets is typically not uniform over the whole area of the magnet. Therefore, it is important to reach a compromise in order to have multiple sensing elements with good sensitivity while keeping high magnetization of the labels that produces externally observable signals.

Chícharo et al. [19] designed and proposed a permanent magnet geometry to generate an out-of-plane external field above 0.1 T with minimal field component in the other directions (< 1 mT). This was achieved throughout a large spatial area of 2 × 6.5 mm^2, where the sensing elements can be located. The authors claimed that when using the customized magnet, all the sensors maintain their characteristics [19]. A group at Siemen Healthcare GmbH proposed the use of a commercial permanent magnet that is positioned below the GMR sensor in a coil setup to minimize magnetic field components of the external permanent magnet in the plane of the sensor [18]. However, a coil setup is usually bulky, hampering system portability. A strategy to overcome the use of external large coils is on-chip fabrication of integrated structures, for the same purpose such as excitation coils reported by Boser and Murali [30] and Murali et al. [26].

Sensor layout and architecture

In the kernel of the magnetic detection system is the sensor unit, i.e., the detection element. Therefore, one of the key development steps of an MFC system is the proper selection and design of the integrated magnetometer. This task consists of a trade-off analysis between the sensor's most important characteristics (e.g., sensitivity and SNR) and emerging differentiation factors (e.g., integration feasibility, miniaturization, low-cost fabrication). For example, unprecedented subpicomolar sensitivities in the measurement of ferromagnetic 30-nm nanoparticles were achieved by implementing a spin-exchange relaxation-free (SERF), optically pumped atomic magnetometer [8]. However, to match low cost, integrated microfluidic platforms for PoC devices, GMR-based sensors are the sensing technology of choice [13, 16].

The detection mechanism in MFC platforms is identical regardless of the sensor type used. As a result, the design process has fundamental guidelines based on the constraints and particularities of in-flow magnetic detection. MFC entails the measurement of the stray fields (magnetic field dipoles) of the magnetic labeled entities flowing within a microfluidic channel (Fig. 1). Successful detection of such entities requires the microfluidic channel to be aligned over the sensor unit, with a layout that considers the sensing direction of the particular magnetic sensor. Various works employing spin valve sensors [5, 25, 33] select rectangular stripes as the sensor's geometry. In this case, the sensing direction is perpendicular to the length of the sensor, which must coincide with the flow direction and thus with the length of the microfluidic channel.

Additionally, the size of the sensing element must be carefully chosen on the basis of the size of the objects of interest, simultaneously ensuring a high sensitivity and the measurement of all particles flowing inside the channel.

Furthermore, the accuracy of the detection is also intimately related to the design of the microfluidic system, particularly the channel dimensions, which are limited not only by the fabrication techniques in use but also dependent on the type of sample and size of target analytes. Even for pure, low viscosity samples (e.g., water, buffer) and smaller targets (from nanometers up to a few micrometers), the dimensions of the channel must be kept several times larger than the targets to avoid clogging, minimize fluidic resistance, and keep the time of analysis short to aid high throughput [35].

Given that it is critical to reduce the size of the microfluidics, and to facilitate the detection of flowing small entities in a relatively large channel, approaches

based on the sensors' architecture have been developed. Some authors have chosen to design sensing elements matching the channel dimensions (Fig. 10a) [33]. This approach guarantees that all targets pass over the sensors. An alternative design, typically used in ferrofluidic droplet detection systems, consists in a meander shape that greatly enlarges the sensing area (Fig. 10d) [10, 21]. However, there is always a trade-off between the size of a sensor and its parameters. Sensor size dictates both spatial resolution and the sensitivity to weak point-like magnetic sources (e.g., individual magnetic particles) [54]. Therefore, a way to overcome the usage of larger sensors is to combine sets of smaller sensors arranged in series in such a way that together they cover the entire channel width (Fig. 10b) [34] or, individual sensors disposed in a step-like configuration (Fig. 10c).

However, data analysis coming from sets of sensors arranged close, side by side, is not trivial, mainly because the same target entity may afford a detection signal on two or more adjacent sensors, making it difficult to distinguish repeated counts from independent events. In this context, hydrodynamic approaches, similarly to the standard flow cytometry, have been explored to focus the sample over the sensing area. The first explored strategy was lateral hydrodynamic focusing [19, 28, 35]. The objective is to narrow down the sample stream to about the target size such that the target can flow in series rather than side by side when passing through the sensing element, ensuring the accuracy of counting. It was found that restricting the transverse range of cell flow by lateral focusing afforded more accurate and reproducible results [28]. However, in MFC, the magnetic signal that reaches the sensor is often reduced as a result of magnetically labeled entities flowing at different heights from the sensor (10–200 μm) inside the microfluidic channels, in this way reducing the detection signal output according to Eq. 3 (Sect. "Magnetic labels") and Eq. 4, as shown in Fig. 11.

$$\Delta V = S\, R_{\min}\, I\, B_x \tag{4}$$

where B_x is the in-plane magnetic stray field of the particle, ΔV is the sensor voltage variation, S is the sensitivity of the sensor, $R_{\min}$ is the minimum resistance of the sensor and I is the biasing current.

In the present example, the sensor is a spin valve of rectangular shape, 2 × 100 μm^2, and a sensitivity ($S\,R_{\min}$) of 2 Ω/mT under a biasing current of 1 mA. A microfluidic channel of 10 μm height and a magnetic particle of 2.8 μm in diameter (Dynabeads M-280 streptavidin) with 4.3 × 10^{-14} A m^2 magnetic moment were considered for the simulation.

In this particular example, particles flowing on the top part of the channel would be barely sensed taking into consideration the noise level of the detection system.

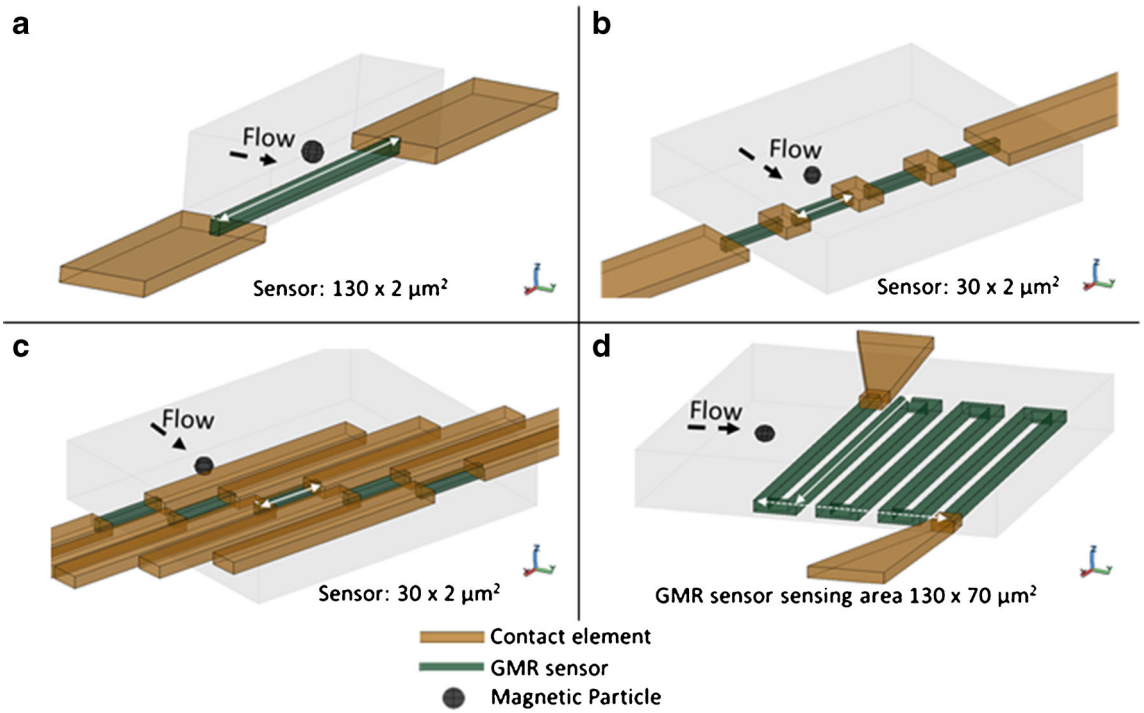

Fig. 10 Schematic illustrating different possible configurations of GMR sensors. **a** A single sensor with its length equal to channel width; **b** an array of 4 sensing elements arranged in series; **c** a set of 5 sensors in a parallel configuration disposed in steps configuration; **d** a sensor patterned in a meander shape

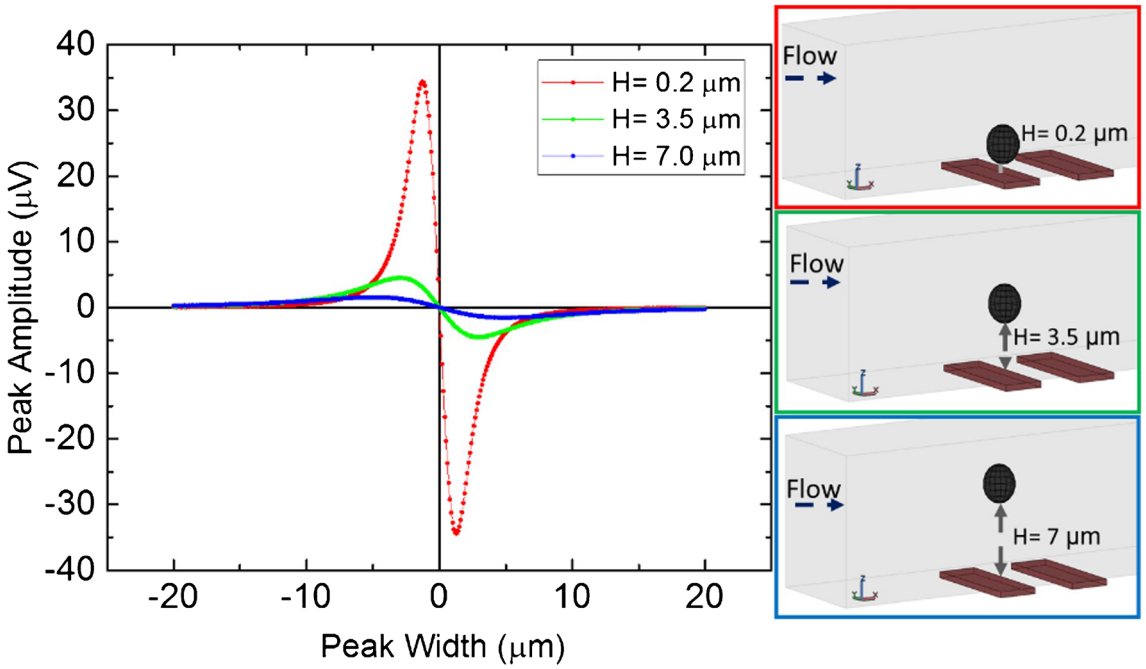

Fig. 11 Signal simulation for a single magnetic particle of 2.8 μm diameter (Dynabeads M-280 streptavidin), and 4.3×10^{-14} A m^2 magnetic moment at a distance (*H*) of 0.2, 3.5, and 7 μm from the sensor

Two complementary strategies may be used to address this issue: (i) improve sensor performance (increase sensitivity, reduce noise) or (ii) bring the flowing entities closer to the sensor (vertical focusing).

Sensor performance

In flow cytometry, a practical definition of "sensitivity" is the capability of the system to resolve subpopulations of cells, e.g., how weakly marked a cell can be and still be resolvable from another population [55]. This capability in optical flow cytometry (OFC) is limited in part by the amount of background light intensity intrinsic to other components in the biological sample (autofluorescence). Conversely, magnetic sensing takes advantage of the nonexistent magnetic background of biological samples. Therefore, MFC can be applied even to turbid or more complex samples since it is not affected by their inherent properties. Nevertheless, in some MFC configurations, the presence of unconjugated magnetic labels (in excess in the labeling process) may contribute to this background noise. Moreover, in magnetic sensing the sensors only detect magnetically labeled events that pass in their proximity. Therefore, target attraction and focusing strategies can be used to allow increased sensitivity and reliability (see next section).

One approach to improving device performance (i.e., sensitivity and reliability) consists in arranging magnetic sensors in a Wheatstone bridge configuration. This geometry, which provides a differential, offset-free output, presents several important advantages for flow cytometry, namely it (i) cancels the common mode signal, reducing the impact of environmental disturbances and noise, such as temperature drifts (of particular interest when working with biological samples) or background magnetic fields and gradients; (ii) enables the use of balance/null measurement method, maximizing the capability of amplification of the output signal; and (iii) delivers characteristic peak patterns of magnetic entities, enabling quantitative analysis. Existing literature reports a vast portfolio of MR sensors implemented in a Wheatstone bridge configuration [15, 18, 21, 28, 51, 56], demonstrating its suitability for high precision measurements, critical for the detection of small output variation caused by in-flow magnetic labeled species.

Lee et al. [28] designed a GMR biosensor for magnetic cell detection also capable of sorting cells with different magnetic moments. In this case, the sensor unit consisted of a single Wheatstone bridge composed of four circular GMR discs (250 μm), one of them being crossed by a microfluidic channel (the active sensor). A background noise signal 3.2 smaller was reported using a Wheatstone bridge configuration when compared with a single GMR disc (without the use of any filter). These authors further highlighted the advantage of this geometry by linking the reduced average noise amplitude obtained with the possibility of distinguishing cells covered with a different number of MNPs.

Several authors have explored the capability of probing the magnetic fingerprint offered by the Wheatstone bridge configuration and combined it with time-of-flight (TOF) analysis to perform quantitative flow cytometry. Reisbeck et al. [27] thoroughly described the detection mechanism of a single cell and spatial resolution of a Wheatstone half-bridge comprising two

GMR sensors. The authors showed that a characteristic four-peak pattern is expected and drew layout considerations claiming that with a cell size to half-bridge ratio > 1.5, binary information can be derive. Applying TOF analysis and using the distance between sensors in the layout as input, this work delivers quantitative single particle information, such as volumetric and immunomagnetic binding capacity.

Helou et al. [51] discussed characteristic signal patterns of magnetic labeled cells using different bridges layouts (comprising 2 × 30 μm^2 GMR stripes): (i) a diagonal half-bridge layout results in a signal with alternating peaks (Fig. 12) and (ii) parallel layout combining two pairs of parallel GMR sensors results in a signature six-peak signal pattern. The authors demonstrated that TOF measurements are suitable to extract cell diameters and that both bridge layouts can be used for cell detection, concluding that a full-bridge delivers higher signal-to noise ratio while a half-bridge provides higher throughput (Fig. 12).

Target vertical focusing

An important aspect of the development of microcytometers is the control of the flow (e.g., velocity, stream location) of target entities inside the microchannels. Sample focusing significantly improves signal quality by making the particles pass precisely over the sensing region [57, 58].

Wolff et al. were the first group to implement a hydrodynamic focusing strategy in microfluidic chips [59]. Since then, reported advantages include allowing the use of channel dimensions large enough to prevent clogging, improvement of detection limits by sharp sample focusing in both the vertical and the horizontal dimension, and suitability to count single cells once these approaches cause particles to flow in single file.

In this context, the 3D hydrodynamic focusing concept was adopted by MFC technology [5, 35]. Here the lateral sheath flows (lateral focus), which drive the sample towards the center of the channel, are combined with a vertical sheath flow (vertical focus) that pushes the sample towards the bottom of the channel. In this way, the targets flow closer to the sensing elements. The authors claim that the vertical focusing increased signal amplitude and enhanced discrimination of labeled cells from free labels [5]. Issadore et al. were able to observe the signal from a single bacterium cell that was not detected without the focusing strategy [35].

However, the major drawback of hydrodynamic focusing is the increase of size and volume of the whole system. It needs a continuous pumping of liquid sheath at high flow rates to generate a thin sample stream.

Another common approach for target pull-down and sorting towards the sensing areas is based on magnetophoretic focusing, which consists in the movement of the targets actuated by magnetic forces in a medium. According to Newton's second law, the translational magnetophoresis of a magnetic particle or a labeled target is described by the following equation:

$$w\frac{\mathrm{d}^2r}{\mathrm{d}^2t} + 3\pi D\eta\frac{\mathrm{d}r}{\mathrm{d}t} - \sum F(r) = 0 \quad (5)$$

where r is the position coordinate of the particle, w is the mass of the magnetic particle, t is the time, and $\sum F(r)$ is the sum of all forces, except the hydrodynamic drag force [60].

Micromagnetic structures, either elements made of ferromagnetic materials or current conductors, are employed for magnetic sorting.

In Loureiro et al.'s study [4], the fluidic platform consists of two microchannels implemented in an H-shaped geometry. The channels are separated by a central wall comprising several gaps to enable the magnetic particles to pass from one channel to the other. To aid in the magnetic separation of labeled cells from unlabeled cells, two successive current conductor metallic lines, crossing the wall gap, were integrated in the detection chip. The magnetic gradient created by these lines is responsible for the

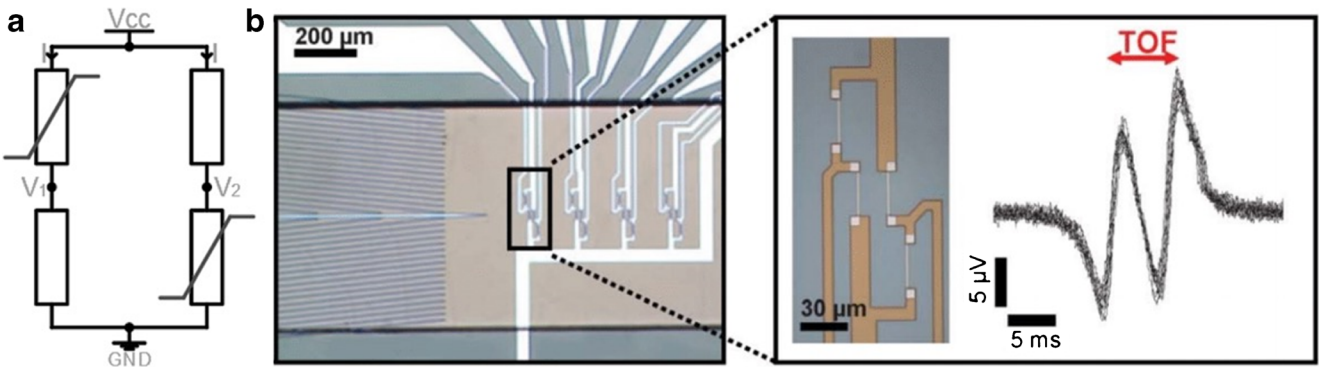

Fig. 12 **a** Schematic of a half-bridge circuit, with a diagonal configuration (transfer curve overlap indicates sensing elements, remaining are reference sensors). **b** Image of integrated MFC chip comprising 4 half Wheatstone bridges overlapped by a microfluidic channel. The zoomed image shows an individual Wheatstone bridge and the superimposed signal from 15 detection events. Adapted from Helou et al. [51]. Reproduced by permission of The Royal Society of Chemistry

magnetophoretic separation of the magnetic particles flowing inside the microchannels.

Also, Jiang et al. [56] reported a device which includes a forked microfluidic channel, flanked by independent tapered current lines for particle sorting. However, it is mentioned that for attraction of beads by the current lines, there is a critical velocity, which is above the bead's Brownian drift velocity. It is also important to bear in mind that electrical structures consume a considerable amount of energy and the Joule heating in the microfluidic channel should be considered in the device design.

Additionally, there are authors taking advantage of magnetic forces coming from a permanent magnet below the chip, which pulls the beads closer to the sensor surface, acting as vertical magnetophoresis [18, 26]. A group at Siemens Healthcare GmbH proposed the combination of those vertical magnetophoretic forces with mechanical focusing structures (like chevrons) in a 3D patterned microfluidic channel (including various enrichment sections) [18]. In this way, balancing hydrodynamic forces and magnetophoretic guiding, an adaptive in situ target enrichment was achieved while eliminating the need for additional sheath-flow focusing strategies.

Ferrofluidic droplets

The detection of ferrofluid droplets, which is extremely relevant for a variety of applications, e.g., drug design and screening or in vivo MRI analysis, has also been profiting from optimized layouts developed for in-flow sensing. As for the case of individual magnetic labeled species, various analyses and magnetic sorting of ferrofluid droplets have been enabled by the capability of extracting their magnetic signal footprint. Pekas et al. [17] reported the detection of a pattern of droplets using an integrated droplet formation T-junction microfluidic system comprising three sets of Wheatstone half-bridges of 4 × 20 μm^2 spin valve GMRs sensors. The flow velocity, droplet size, and droplet-formation frequency were successfully determined from the characteristic sensor response. In the design of GMR-based MFC platforms for droplet dictation, there are also geometrical constraints concerning sensor and droplet dimensions to avoid sensor saturation occurring when the sensor width is equal to the length of the droplet [15]. Later, the same group further explored this feature and demonstrated a magnetic encoding concept for droplet microfluidic systems [10]. GMR multilayer sensors arranged in a meander shape were selected as a magnetic decoding element and mounted in a single Wheatstone bridge configuration using three off-chip trimmers. The implementation of a meander shape composed of 19 turns of 3 × 100 μm^2 GMR stripes allowed the sensor to have an enlarged active area of approximately 100 × 100 μm^2. Additionally, this meander shape of magnetic sensors is often used owing to its well-defined orientation of sensitive layer combined with an increased sensor length, which in turn enables a higher resistance variation, thereby increasing the sensor sensitivity [21].

More exquisite strategies have been proposed aiming at enhanced detection of magnetic markers' stray fields by the magnetic sensors. Flexible sensors have been proposed in the format of a rolled-up GMR-based magnetic sensor [21] and flexible polymer-sandwiched GMR [13] being prominent examples. Mönch et al. [21] combined GMR multilayer sensors with meander shapes arranged in a Wheatstone half-bridge configuration discussed earlier. The authors claimed that for a particle magnetized along the flow direction, the fringe field produced can be detected in all directions by a GMR sensor with a tubular shape. Lin et al. [13] developed a flexible microfluidic device equipped with in situ magnetic functionality, which when associated with MNPs is used to enrich biomarkers to the near-skin area to enhance the detection.

These approaches, in addition to potentially increasing the sensitivity of detection, also pave the way for the development of wearable and/or implantable solutions based on integrated magneto-fluidic sensors—a key future trend for MFC systems.

Electronics interface

When designing a sensor interface and signal processing system for MFC, adequate signal bandwidth, and consequently the acquisition rate, both influenced by the flow speed, sensor shape and size, particle size and number, and event frequency, must be determined. Additional important information is the sensor signal intensity and the SNR of the acquisition chain.

Signal-to-noise ratio

An important constraint in the design of the electrical interface is the system noise, and consequently the SNR. To increase the SNR three major actions can be taken: (i) increase the signal intensity, (ii) reduce system noise, (iii) or reduce the bandwidth to integrate less noise.

Increasing the signal intensity mainly depends on the sensors which are the source of the signal (described in Sects. "Sensing technologies for magnetic cytometry" and "Sensor layout and architecture"). Reducing the system noise depends mainly on the biasing architecture and the first amplification stage. For the resistive/impedance sensors, most of the works use very simple and reliable biasing schemes like Wheatstone bridges [10, 11, 13, 17, 21, 23, 24, 51, 56] or half-bridge [22, 27, 34], or benchtop current sources [16, 31, 35]. The amplification/acquisition of the signal is in most cases performed with ultra-low noise benchtop lock-in amplifiers, high precision voltmeters, or with custom-built discrete electronics [5, 31, 33, 35].

Bandwidth

The correct determination of the acquisition bandwidth of the system is paramount. It should be noted that the bandwidth is dependent on the event duration and shape, which is related to particle size, proximity to the sensor, and flow speed [27, 61, 62]. However, when using commercial undedicated electronics, the bandwidth is mostly defined by the sampling rate of the available analog to digital converter (ADC) to avoid anti-aliasing, and the flow speed and event frequency of the experiment are adapted to the hardware [9, 27, 28, 62].

The use of commercial devices is a reasonable choice because it is challenging and time consuming to replicate the performance of these amplifiers in a custom-made system. The lock-in amplifier limits the bandwidth to the minimum possible, reducing the integrated noise and increasing the SNR, although to use it the particles must be magnetized by an external AC field. The frequency of this AC field should be much higher than the event duration and frequency. However, if the target is to reach a PoC device, such all-purpose devices must be replaced by custom-tailored analog front ends [33], and ADCs.

Most works measure the sensor signal in the baseband sampling at low rates (< 200 ksps), while some use larger sampling frequencies [31] to allow for lower test times, sacrificing the noise performance.

Signal processing and peak detection

Regarding signal, most works use digital or analog bandpass filtering to reduce noise. However, Huang et al. [61] presented a matched filter, which according to the authors, increases the SNR by four-fold.

The detection principles are mostly based on peak threshold detection and heuristics. The pulses are fed to a decision algorithm that evaluates if the number of threshold matches what is expected [5, 27, 61]. The most complex systems [27, 61] use the simulated results of the MNP/sensor interaction to predict the expected pulses.

Sensor multiplexing

To address more than one sensor, one either multiplies the number of interfaces by the number of sensors, which rapidly increases the complexity of the interface, or uses multiplexing techniques and schemes at some point in the interface. In Duarte et al. [33] this multiplexing is done at the end of the analog chain by using a multiplexed digital acquisition board (Fig. 13).

In works related to steady state magnetic detection systems, it has been shown that it is possible to perform this multiplexing before the amplification stage by integrating CMOS chips as the analog interface [63, 64]. Using CMOS grants a lot of flexibility, scalability, and area efficiency when interfacing sensors, scaling up the number of sensors from dozens to hundreds or even thousands of sensors.

In the case of dynamic/flow measurement, the duration of the event, i.e., the time the particles are interacting with the sensors, is inversely related to the bandwidth, which means that short events have large bandwidths. Since the progress is also in the direction of the reduction of test times, this means that bandwidths tend to increase. Thus, when designing a multiplexed interface, both acquisition frequencies and even data transfer rates will be challenging, and the approach will probably rely on bringing the processing of raw data closer to the sensors and transmitting to the user only the events or event-related information.

Conclusions and future trends

This review gives an overview of the current research on magnetic flow cytometry. Although less advanced than the established optical flow cytometry technique, MFC is presented as a promising approach, particularly with respect to its compatibility with miniaturized assay formats, prompting the development of lab-on-chip platforms. The article discusses the technology based on its main components, namely (i) the sensing units, their performance, and reported architecture; (ii) magnetic labels; (iii) fluidic design; and (iv) electronic signal processing.

Different magnetic sensors have been identified to measure the average fringe field of magnetic entities flowing over the sensing area. The principle of operation and the intrinsic properties of magnetic sensors such as sensitivity are important aspects to consider. In this context, it is noted that magnetoresistive sensors, particularly spin valve (SV) sensors, are the most reported sensors in the literature. Although having lower sensitivity when compared to PHE or MTJs (Table 3), their high magnetoresistance and minimum noise contribution from the electronic acquisition systems make them the preferred choice for MFC applications. The sensor size dictates both spatial resolution and the ability of the system to detect individual magnetic events. Different sensor geometries have been identified in the current work, highlighting a great versatility in the microfabrication process of magnetic sensors. Of note is the ability to tune the sensor's size according to the target analytes of interest, as a measure to increase assay sensitivity.

Magnetic labels and respective magnetic moments are important elements to consider. Most works use superparamagnetic particles as the labels of choice, particularly smaller labels (1–100 nm), which are expected to allow for higher labeling densities of the analytes of interest. Additionally, the ability to adequately functionalize the particles with recognition elements, such as antibodies, must be

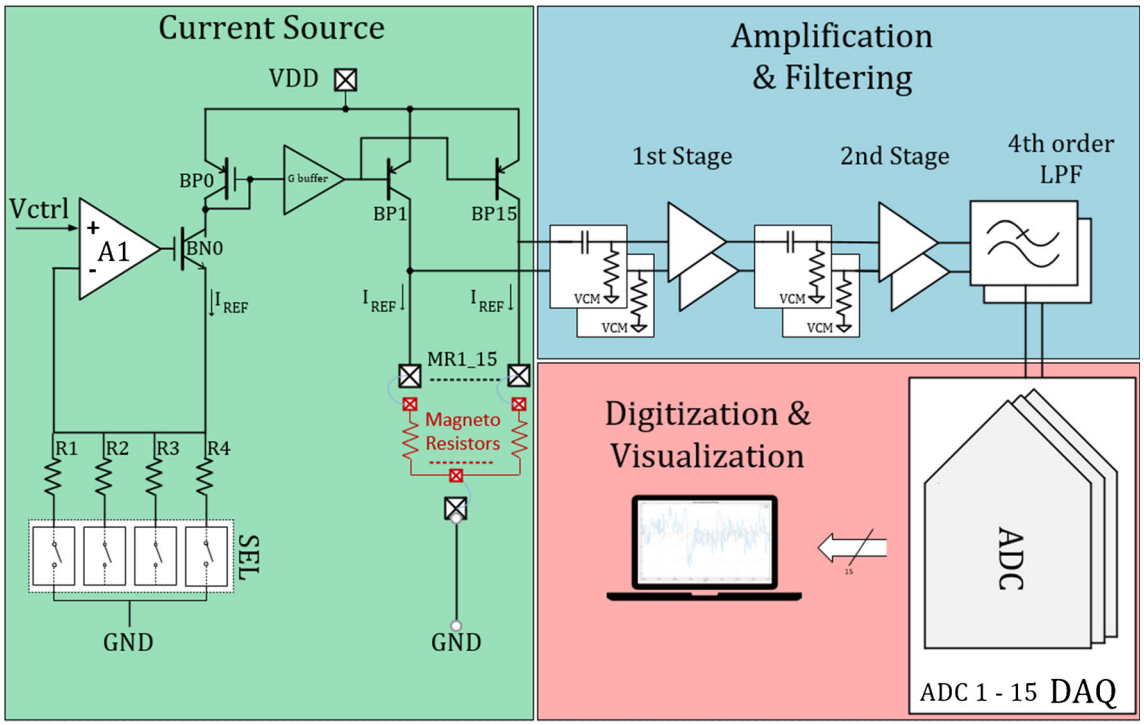

Fig. 13 Schematic representation of the electronics for sensor biasing and signal acquisition

considered. Some works reported standard commercially available particles while others tailored the particles according to their needs. Ultimately, the type of particles, the type and quality of the recognition element, and respective immobilization chemistry impact assay sensitivity and specificity.

The coupling of microfluidic channels with the sensing units is an essential requisite in the identified literature. The channel networks not only allow for sample flowing over the sensing area and automation but also impact the assay sensitivity. Channel dimensions are usually kept larger than the targets to avoid clogging and minimize fluidic resistance. However, signal intensity is inversely proportional to the distance from the sensors; therefore, a careful choice of the channel size is of paramount importance. Target focusing emerges as viable approach to simultaneously focus the label targets over the sensing area while overcoming the constraints of restricted channel dimensions.

As mentioned earlier, electronic signal acquisition has a major impact on SNR of the system. Therefore, the correct determination of the bandwidth of the system is paramount. Most of the reported works use commercial undedicated electronics that most of the time hamper the full miniaturization of the system.

While in steady state magnetic detection systems, integrated electronics and scalability are at an advanced stage, it is still challenging to address the dynamic flow measurement characteristics such as particle velocity and proximity of the sensors, which both influence the typical peak signal length and shape.

Despite the recognized capabilities of MFC technology, several important challenges need to be addressed before these systems achieve their full potential as integrated systems capable of moving from the laboratory into a real-world application. Indeed, most of the reported works deal with simulated laboratorial samples.

Additionally, minimum hands-on time, automated sample processing, affordable price, and sensitivity and specificity comparable to standard assays are milestones that are yet to be achieved.

The automated handling of samples can be accomplished with the integration of microfluidics which is well described in several MFC systems. Nevertheless, in most cases, PDMS is the material of choice. The simple fabrication method and easiness of replication make this polymer useful for small-scale production, yet impractical for a cost-effective scale-up. Undoubtedly, the introduction of other polymers such as those provided by micromachining plastics or channels based on pressure-sensitive adhesives may provide a cost-saving approach for the fluidic system.

Another sensitive aspect relates to sample volumes and relevant concentrations of the target analytes. As microfluidic technology evolves, femtoliter to nanoliter volumes can now be manipulated in an automatic manner. Nevertheless, such small volumes may induce sampling errors or demand for a long analysis time to provide statistically accurate results. Magnetic manipulation is an implicit advantage of using magnetic tags, as it provides a means for separation and/or focusing of the labeled targets. Besides simplifying the sample

preparation step and enhancing the detection limit by in situ target concentration, magnetic labeling offers the possibility of manipulating and positioning the labeled targets directly above the sensing elements for increased measurement accuracy. Some of the described techniques rely on the use of external magnetic fields provided by either permanent magnets, coils, or patterned magnetic films. Used alone, or in combination with hydrodynamic focus, the exploitation of such structures has been proven successful to overcome some of the constraints on detection limits.

As MFC platforms evolve, the possibility of the simultaneous detection of different biomarkers will become an important requirement. In this context, some groups are exploiting distinct particle signatures for differential labeling of target cells. For example, Issadore et al. [31] used different particles exhibiting distinct magnetization properties to target different biomarkers in the same cell. The easiness of integration of some magnetic sensors, notably GMR sensors, with flexible/stretchable substrates eliminates the constraint of planar substrates. In view of this, tubes and capillaries can be shaped with sensing capabilities. Ultimately, these new configurations may allow for the in vivo monitoring of flowing labeled markers and pharmacodynamic studies. Finally, the defined manipulation of ferrofluids provided by certain MFC systems will offer new opportunities for imaging and may extend MFC applications beyond the biological scope.

Acknowledgements This work has received funding from European Structural & Investment Funds through the COMPETE Program and from National Funds through FCT – Fundação para a Ciência e a Tecnologia under the grants SAICTPAC/0019/2015, MUSIC-PESSOA 2017-38027RF and MagScopy4IHC- LISBOA-01-0145-FEDER-031200. The authors acknowledge funding from the European Union through the project MAGNAMED- H2020-MSCA-RISE-2016 grant n. 734801. The authors R. Soares, D. M. Caetano and P. H. Fonseca, acknowledge their PhD grants, PD/BD/128205 /2016, PD/BD/128208/2016, PD/BD/135272/2017, respectively, funded through the Advanced Integrated Microsystems (AIM) doctoral program.

Compliance with ethical standards

No experiments involving human participants and/or animals have been conducted for this publication.

Conflict of interest The authors declare that they have no conflict of interest.

Publisher's note Springer Nature remains neutral with regard to jurisdictional claims in published maps and institutional affiliations.

References

1. Moldavan A. Photo-electric technique for the counting of microscopical cells. Science. 1934;80:188–9.
2. Hejazian M, Li W, Nguyen N-T. Lab on a chip for continuous-flow magnetic cell separation. Lab Chip. 2015;15:959–70. https://doi.org/10.1039/C4LC01422G.
3. Plouffe BD, Murthy SK, Lewis LH. Fundamentals and application of magnetic particles in cell isolation and enrichment. Rep Prog Phys. 2015;78:16601. https://doi.org/10.1088/0034-4885/78/1/016601.
4. Loureiro J, Fermon C, Pannetier-Lecoeur M, Arrias G, Ferreira R, Cardoso S, et al. Magnetoresistive detection of magnetic beads flowing at high speed in microfluidic channels. IEEE Trans Magn. 2009;45:4873–6. https://doi.org/10.1109/TMAG.2009.2026287.
5. Chícharo A, Martins M, Barnsley LC, Taouallah A, Fernandes J, Silva BFB, et al. Enhanced magnetic microcytometer with 3D flow focusing for cell enumeration. Lab Chip. 2018;18:2593–603. https://doi.org/10.1039/C8LC00486B.
6. Tasadduq B, Lam W, Alexeev A, Sarioglu AF, Sulchek T. Enhancing size based size separation through vertical focus microfluidics using secondary flow in a ridged microchannel. Sci Rep. 2017;7:17375. https://doi.org/10.1038/s41598-017-17388-w.
7. Zhao Y, Li Q, Hu X. Universally applicable three-dimensional hydrodynamic focusing in a single-layer channel for single cell analysis. Anal Methods. 2018;10:3489–97. https://doi.org/10.1039/C8AY01017J.
8. Bougas L, Langenegger LD, Mora CA, Zeltner M, Stark WJ, Wickenbrock A, et al. Nondestructive in-line sub-picomolar detection of magnetic nanoparticles in flowing complex fluids. Sci Rep. 2018;8:3491. https://doi.org/10.1038/s41598-018-21802-2.
9. Fodil K, Denoual M, Dolabdjian C, Treizebre A, Senez V. In-flow detection of ultra-small magnetic particles by an integrated giant magnetic impedance sensor. Appl Phys Lett. 2016;108:173701. https://doi.org/10.1063/1.4948286.
10. Lin G, Karnaushenko DD, Bermúdez GSC, Schmidt OG, Makarov D. Magnetic suspension array technology: controlled synthesis and screening in microfluidic networks. Small. 2016;12:4553–62. https://doi.org/10.1002/smll.201601166.
11. Lin G, Makarov D, Medina-Sanchez M, Guix M, Baraban L, Cuniberti G, et al. Magnetofluidic platform for multidimensional magnetic and optical barcoding of droplets. Lab Chip. 2015;15:216–24. https://doi.org/10.1039/c4lc01160k.
12. Kim KW, Reddy V, Torati SR, Hu XH, Sandhu A, Kim CG. On-chip magnetometer for characterization of superparamagnetic nanoparticles. Lab Chip. 2015;15:696–703. https://doi.org/10.1039/C4LC01076K.
13. Lin G, Makarov D, Melzer M, Si W, Yan C, Schmidt OG. A highly flexible and compact magnetoresistive analytic device. Lab Chip. 2014;14:4050–8. https://doi.org/10.1039/c4lc00751d.
14. Fodil K, Denoual M, Dolabdjian C, Harnois M, Senez V. Dynamic sensing of magnetic nanoparticles in microchannel using GMI technology. IEEE Trans Magn. 2013;49:93–6. https://doi.org/10.1109/TMAG.2012.2218797.
15. Lin G, Baraban L, Han L, Karnaushenko D, Makarov D, Cuniberti G, et al. Magnetoresistive emulsion analyzer. Sci Rep. 2013;3:2548.
16. Melzer M, Karnaushenko D, Makarov D, Baraban L, Calvimontes A, Mönch I, et al. Elastic magnetic sensor with isotropic sensitivity for in-flow detection of magnetic objects. RSC Adv. 2012;2:2284–8. https://doi.org/10.1039/C2RA01062C.
17. Pekas N, Porter MD, Tondra M, Popple A, Jander A. Giant magnetoresistance monitoring of magnetic picodroplets in an integrated microfluidic system. Appl Phys Lett. 2004;85:4783–5. https://doi.org/10.1063/1.1825059.
18. Reisbeck M, Richter L, Helou MJ, Arlinghaus S, Anton B, van Dommelen I, et al. Hybrid integration of scalable mechanical and magnetophoretic focusing for magnetic flow cytometry. Biosens

Bioelectron. 2018;109:98–108. https://doi.org/10.1016/j.bios.2018.02.046.
19. Chícharo A, Barnsley L, Martins M, Cardoso S, Dieguez L, Espiña B, et al. Custom magnet design for a multi-channel magnetic microcytometer. IEEE Trans Magn. 2018;54:1–5. https://doi.org/10.1109/TMAG.2018.2835369.
20. García-Arribas A, Martínez F, Fernández E, Ozaeta I, Kurlyandskaya GV, Svalov AV, et al. GMI detection of magnetic-particle concentration in continuous flow. Sensors Actuators A Phys. 2011;172:103–8. https://doi.org/10.1016/j.sna.2011.02.050.
21. Mönch I, Makarov D, Koseva R, Baraban L, Karnaushenko D, Kaiser C, et al. Rolled-up magnetic sensor: nanomembrane architecture for in-flow detection of magnetic objects. ACS Nano. 2011;5:7436–42. https://doi.org/10.1021/nn202351j.
22. Aledealat K, Mihajlović G, Chen K, Field M, Sullivan GJ, Xiong P, et al. Dynamic micro-Hall detection of superparamagnetic beads in a microfluidic channel. J Magn Magn Mater. 2010;322:L69–72. https://doi.org/10.1016/j.jmmm.2010.08.006.
23. Loureiro J, Ferreira R, Cardoso S, Freitas PP, Germano J, Fermon C, et al. Toward a magnetoresistive chip cytometer: integrated detection of magnetic beads flowing at cm/s velocities in microfluidic channels. Appl Phys Lett. 2009;95:34104. https://doi.org/10.1063/1.3182791.
24. Shen W, Liu X, Mazumdar D, Xiao G. In situ detection of single micron-sized magnetic beads using magnetic tunnel junction sensors. Appl Phys Lett. 2005;86:253901. https://doi.org/10.1063/1.1952582.
25. Ferreira HA, Graham DL, Parracho P, Soares V, Freitas PP. Flow velocity measurement in microchannels using magnetoresistive chips. IEEE Trans Magn. 2004;40:2652–4. https://doi.org/10.1109/TMAG.2004.830403.
26. Murali P, Niknejad AM, Boser BE. CMOS microflow cytometer for magnetic label detection and classification. IEEE J Solid-State Circuits. 2017;52:543–55. https://doi.org/10.1109/JSSC.2016.2621036.
27. Reisbeck M, Helou MJ, Richter L, Kappes B, Friedrich O, Hayden O. Magnetic fingerprints of rolling cells for quantitative flow cytometry in whole blood. Sci Rep. 2016;6:32838.
28. Lee C-P, Lai M-F, Huang H-T, Lin C-W, Wei Z-H. Wheatstone bridge giant-magnetoresistance based cell counter. Biosens Bioelectron. 2014;57:48–53. https://doi.org/10.1016/j.bios.2014.01.028.
29. Vila A, Martins VC, Chícharo A, Rodriguez-Abreu C, Fernandes AC, Cardoso FA, et al. Customized design of magnetic beads for dynamic magnetoresistive cytometry. IEEE Trans Magn. 2014;50:1–4. https://doi.org/10.1109/TMAG.2014.2324411.
30. Boser BE, Murali P. Flow cytometer-on-a-chip. In: 2014 IEEE Biomedical Circuits and Systems Conference (BioCAS) Proceedings. Lausanne; 2014. p. 480–483. https://doi.org/10.1109/BioCAS.2014.6981767.
31. Issadore D, Chung J, Shao H, Liong M, Ghazani AA, Castro CM, et al. Ultrasensitive clinical enumeration of rare cells ex vivo using a μ-Hall detector. Sci Transl Med. 2012;4:141ra92. https://doi.org/10.1126/scitranslmed.3003747.
32. Loureiro J, Andrade PZ, Cardoso S, da Silva CL, Cabral JM, Freitas PP. Magnetoresistive chip cytometer. Lab Chip. 2011;11:2255–61. https://doi.org/10.1039/c0lc00324g.
33. Duarte C, Costa T, Carneiro C, Soares R, Jitariu A, Cardoso S, et al. Semi-quantitative method for Streptococci magnetic detection in raw milk. Biosensors. 2016;6:19. https://doi.org/10.3390/bios6020019.
34. Fernandes AC, Duarte CM, Cardoso FA, Bexiga R, Cardoso S, Freitas PP. Lab-on-Chip cytometry based on magnetoresistive sensors for bacteria detection in milk. Sensors (Basel). 2014;14:15496–524. https://doi.org/10.3390/s140815496.
35. Issadore D, Chung HJ, Chung J, Budin G, Weissleder R, Lee H. muHall chip for sensitive detection of bacteria. Adv Healthc Mater. 2013;2:1224–8. https://doi.org/10.1002/adhm.201200380.
36. McGuire T, Potter R. Anisotropic magnetoresistance in ferromagnetic 3d alloys. IEEE Trans Magn. 1975;11:1018–38. https://doi.org/10.1109/TMAG.1975.1058782.
37. van de Veerdonk RJM, Beliën PJL, Schep KM, Kools JCS, de Nooijer MC, Gijs MAM, et al. 1/f noise in anisotropic and giant magnetoresistive elements. J Appl Phys. 1997;82:6152–64. https://doi.org/10.1063/1.366533.
38. Nguyen Van Dau F, Schuhl A, Childress JR, Sussiau M. Magnetic sensors for nanotesla detection using planar Hall effect. Sensors Actuators A Phys. 1996;53:256–60. https://doi.org/10.1016/0924-4247(96)01152-1.
39. Ejsing L, Hansen MF, Menon AK, Ferreira HA, Graham DL, Freitas PP. Planar Hall effect sensor for magnetic micro- and nanobead detection. Appl Phys Lett. 2004;84:4729–31. https://doi.org/10.1063/1.1759380.
40. Damsgaard C, Cardoso S, Freitas P, Hansen M. Exchange-biased planar Hall effect sensor optimized for biosensor applications. J Appl Phys. 2008;103(7):07A302–07A302-3.
41. Freitas P, Ferreira H, Graham D, Clarke L, Amaral M, Martins V, et al. Magnetoresistive biochips E. In: Johnson M, editor. Magnetoelectronics. Amsterdam: Elsevier.
42. Baibich MN, Broto JM, Fert A, Van Dau FN, Petroff F, Etienne P, et al. Giant magnetoresistance of (001)Fe/(001)Cr magnetic superlattices. Phys Rev Lett. 1988;61:2472–5. https://doi.org/10.1103/PhysRevLett.61.2472.
43. Binasch G, Grünberg P, Saurenbach F, Zinn W. Enhanced magnetoresistance in layered magnetic structures with antiferromagnetic interlayer exchange. Phys Rev B. 1989;39:4828–30. https://doi.org/10.1103/PhysRevB.39.4828.
44. Dieny B, Speriosu VS, Parkin SSP, Gurney BA, Wilhoit DR, Mauri D. Giant magnetoresistive in soft ferromagnetic multilayers. Phys Rev B. 1991;43:1297–300. https://doi.org/10.1103/PhysRevB.43.1297.
45. Heim DE, Fontana RE, Tsang C, Speriosu VS, Gurney BA, Williams ML. Design and operation of spin valve sensors. IEEE Trans Magn. 1994;30:316–21. https://doi.org/10.1109/20.312279.
46. Freitas PP, Ferreira R, Cardoso S, Cardoso F. Magnetoresistive sensors. J Phys Condens Matter. 2007;19:165221. https://doi.org/10.1088/0953-8984/19/16/165221.
47. Hayakawa J, Ikeda S, Lee YM, Matsukura F, Ohno H. Effect of high annealing temperature on giant tunnel magnetoresistance ratio of CoFeB/MgO/CoFeB magnetic tunnel junctions. Appl Phys Lett. 2006;89:232510. https://doi.org/10.1063/1.2402904.
48. Graham DL, Ferreira HA, Freitas PP. Magnetoresistive-based biosensors and biochips. Trends Biotechnol. 2004;22:455–62. https://doi.org/10.1016/j.tibtech.2004.06.006.
49. Krieg E, Weissman H, Shirman E, Shimoni E, Rybtchinski B. A recyclable supramolecular membrane for size-selective separation of nanoparticles. Nature Nanotechnol. 2011;6:141–6. https://doi.org/10.1038/nnano.2010.274.
50. Robertson JD, Rizzello L, Avi M, Gaitzsch J. Purification of nanoparticles by size and shape. Sci Rep. 2016;6:27494. https://doi.org/10.1038/srep27494.
51. Helou M, Reisbeck M, Tedde SF, Richter L, Bär L, Bosch JJ, et al. Time-of-flight magnetic flow cytometry in whole blood with integrated sample preparation. Lab Chip. 2013;13:1035–8. https://doi.org/10.1039/c3lc41310a.
52. Martins SSA, Martins VC, Cardoso FA, Freitas PP, Fonseca LP. Waterborne pathogen detection using a magnetoresistive immunochip BT. In: Tiquia-Arashiro SM, editor. Molecular biological technologies for ocean sensing. Totowa: Humana; 2012. p. 263–88.
53. He J, Huang M, Wang D, Zhang Z, Li G. Magnetic separation techniques in sample preparation for biological analysis: a review.

J Pharm Biomed Anal. 2014;101:84–101. https://doi.org/10.1016/j.jpba.2014.04.017.
54. Ripka P, Janosek M. Advances in magnetic field sensors. IEEE Sens J. 2010;10:1108–16. https://doi.org/10.1109/JSEN.2010.2043429.
55. Hoffman RA, Wood JCS. Characterization of flow cytometer instrument sensitivity. Curr Protoc Cytom. 2007;40:1.20.1–1.20.18. https://doi.org/10.1002/0471142956.cy0120s40.
56. Jiang Z, Llandro J, Mitrelias T, Bland JAC. An integrated microfluidic cell for detection, manipulation, and sorting of single micron-sized magnetic beads. J Appl Phys. 2006;99:08S105. https://doi.org/10.1063/1.2176238.
57. Piyasena ME, Graves SW. The intersection of flow cytometry with microfluidics and microfabrication. Lab Chip. 2014;14:1044–59. https://doi.org/10.1039/C3LC51152A.
58. Frankowski M, Theisen J, Kummrow A, Simon P, Ragusch H, Bock N, et al. Microflow cytometers with integrated hydrodynamic focusing. Sensors (Basel). 2013;13(4):4674–93.
59. Wolff A, Perch-Nielsen IR, Larsen UD, Friis P, Goranovic G, Poulsen CR, et al. Integrating advanced functionality in a microfabricated high-throughput fluorescent-activated cell sorter. Lab Chip. 2003;3:22–7. https://doi.org/10.1039/b209333b.
60. Liu C, Stakenborg T, Peeters S, Lagae L. Cell manipulation with magnetic particles toward microfluidic cytometry. J Appl Phys. 2009;105:102014. https://doi.org/10.1063/1.3116091.
61. Huang C, Zhou X, Ying D, Hall DA. A GMR-based magnetic flow cytometer using matched filtering. In: 2017 IEEE Sensors. Glasgow, 2017. p. 1–3. https://doi.org/10.1109/ICSENS.2017.8233892.
62. Sun X, Feng Z, Zhi S, Lei C, Zhang D, Zhou Y. An integrated microfluidic system using a micro-fluxgate and micro spiral coil for magnetic microbeads trapping and detecting. Sci Rep. 2017;7:12967. https://doi.org/10.1038/s41598-017-13389-x.
63. Cardoso FA, Costa T, Germano J, Cardoso S, Borme J, Gaspar J, et al. Integration of magnetoresistive biochips on a CMOS circuit. IEEE Trans Magn. 2012;48:3784–7. https://doi.org/10.1109/TMAG.2012.2198449.
64. Costa T, Cardoso FA, Germano J, Freitas PP, Piedade MS. A CMOS front-end with integrated magnetoresistive sensors for biomolecular recognition detection applications. IEEE Trans Biomed Circuits Syst. 2017;11:988–1000. https://doi.org/10.1109/TBCAS.2017.2743685.